A Novel Method for Generating Tricolor Emission with SnSb Alloy

By

P.Priyanka

(15PPH009)

Thesis submitted to

Avinashilingam Institute for Home Science and Higher Education for Women,

Coimbatore – 641 043

In partial fulfilment of the requirements for the Degree of

Master of Science in Physics

April 2017

A Novel Method of Generating Tricolor Emission with SnSb Alloy

By

Priyanka P

(15PPH009)

Thesis submitted to

Avinashilingam Institute for Home Science and Higher Education for Women

Coimbatore – 641 043

In partial fulfilment of the requirements for the Degree of

Master of Science in Physics

April 2017

CERTIFIED AS A BONAFIDE RESEARCH WORK

10/04/'17

Signature of the Guide

10/4/17

Signature of the Head of the Department

ACKNOWLEDGEMENT

ACKNOWLEDGEMENT

I owe my respectful gratitude and sincere thanks to **Dr. (Thiru.) P.R.Krishnakumar**, Chancellor, Avinashilingam Institute for Home Science and Higher Education for Women, University, Coimbatore-43 for all the amenities provided for the conduct of the project.

I wish to record my heartful thanks to **Dr. (Tmt.) Premavathy Vijayan,** M.Sc., M.Ed., Dip..Spl Edn., M.Phil., Ph.D., Vice Chancellor, Avinashilingam Institute for Home Science and Higher Education for Women, University, Coimbatore-43, for extending all possible help towards the completion of the study.

I record my immense gratitude to **Dr. (Tmt.), S. Kowsalya,** M.Sc., M.Phil., Ph.D., Registrar, Avinashilingam Institute for Home Science and Higher Education for Women, University, Coimbatore, for providing a good opportunity to carry out this piece of work.

I feel greatly indebted and thankful **to Dr. (Tmt.) A. Parvathi**, M.Sc., and Dip.Ed., M.Phil., Ph.D., Dean, Faculty of Science, Avinashilingam Institute for Home Science and Higher Education for Women, University, Coimbatore, for her continued interest and valuable guidance in the conduct of this project.

I wish to express my sincere thanks to **Dr. (Tmt.) Saroja Prabakaran**, M.Sc., Dip.Ed., M.Phil., Ph.D., Former Vice Chancellor, The Hall of Residence, Warden, Avinashilingam Education Trust Institutions Hostel, Coimbatore, for her generous help, grateful support and meticulous care provided for carrying out this work successfully.

I wish to record my sincere thanks to **Dr.(Tmt.) J. Shanthi**, M.Sc., M.Phil., Ph.D., Associate Professor, Professor and Head of the Department of Physics, Avinashilingam Institute for Home Science and Higher Education for Women, University, Coimbatore, for her encouragement and generous help which was of great value.

I am very much obliged to record my deep sense of gratitude and indebtedness to my respectful guide **Dr.(Tmt.) B. Nalini,** M.Sc., Ph.D., M.S (Edu.Mgt.), STA fellow, AIST Fellow (Japan), Assistant Professor, Avinashilingam Institute for Home Science and Higher Education for Women, University, Coimbatore, for her valuable guidance learned counsel, cordial treatment, keen interest, constant encouragement and care rendered throughout the course of my investigation.

I feel very grateful to deliver my gratitude to **Dr. A. Chandra Bose**, Associate Professor, Nanomaterials Laboratory, Department of Physics, National Institute of Technology, Trichy for rendering ideas, technical support and encouragement.

I wish to place my deep sense of gratitude to **Dr. (Mrs.) S.Subhashini**, Professor, M.Sc., M.H.Ed., M.Phil., Ph.D., Avinashilingam Institute for Home Science and Higher Education for Women, University, Coimbatore for her support in providing essential means of help for completion of thermal characterizations in my study.

I also extend my sincere thanks to **all the staff members** of the Department of Physics for their direct and indirect support for carrying out this work.

On a personal note, I express my deep sense of gratitude to my **Parents**, brother and my friends for their support, encouragement, moral and physical assistance rendered by them throughout the course of my study.

Above all I humbly thank the **God Almighty** for immense mercy for the successful completion of my work.

P.PRIYANKA

CONTENT

CONTENT

III	**MATERIALS AND METHODS**
	3.1 Introduction
	3.2 Nanoparticle synthesis
	3.3 Synthesis Techniques
	3.4 Co-precipitation method
	3.4.1 Advantages of co-precipitation
	3.4.2 Synthesis of Copper sulphide by co-precipitation method
	3.4.3 Raw materials used
	3.5 Experimental details
	3.5.1 Preparation of Copper Sulphide
	3.5.2 Preparation of tin antimony alloy
	3.5.3 Preparation of pulverized CuS : Sn_2Sb_3
	3.6 Characterization Techniques
	3.6.1 X-Ray Diffraction (XRD)
	3.6.2 Thermal Analysis
	3.6.2.1 Thermal Gravimetric Analysis (TGA)
	3.6.2.2 Differential Thermal Gravimetric Analysis (DTG)
	3.6.3 Fourier Transformation Infrared Spectroscopy
	3.6.4 Scanning Electron Microscope (SEM)
	3.6.5 Energy Dispersive X-ray Analysis (EDX)
	3.6.6 Ultra Violet-Visible Spectroscopy (UV-Vis)
	3.6.7 Photoluminescence (PL)

LIST OF FIGURES

LIST OF TABLES

INTRODUCTION

CHAPTER I

INTRODUCTION

1.1 Phosphor

Semiconductor lighting technology is one of the most priority fields of science andtechnology in many developed countries. The main device employing semiconductor lighting structures is a light emitting diode (LED) [1]. The process of phosphorescence exhibits continuous emission of radiation for a longer period after the excitation radiation ceases. Phosphor is a substance which converts absorbed energy into emitted light. In recent years, it remains as a significant progress in the development of optical storage phosphors and materials for light emitting purpose. One of the current research topics includes the study of phosphor material for white light emitting purpose. White light-emitting diodes (w-LEDs) have attracted considerable attention in solid-state lighting area due to their superior properties, such as high energy efficiency, stability, long lifetime and environmental friendliness, compared to conventional incandescent and fluorescence lamps [2]. Today's most common approach for white light-emitting diodes relies on a combination of blue LED light and a phosphor material emitting green and red or both together or separate.

An overwhelming role has been made to the development of phosphors in Phosphor coated-White LEDs (pc-WLEDs) with the adventure of science and technology, such as micro and nano-solid material synthesis, functionalisation and characterization of materials, as well as the emergence of novel luminescent materials. Major challenges in pc-WLEDs until now have been to achieve high luminous efficacy, high chromatic stability, brilliant colour-rending properties, and price competitiveness with fluorescent lamps, which rely critically on the phosphor properties. An intensive understanding of the nature and limitations of phosphors and the factors dominating the general trends in pc-WLEDs is essential for advancing technological applications.

1.2 History of Phosphors

The applications of phosphors were known to mankind for more than 2000 years ago. Prior to the discovery of bolignion stone, the Japanese successfully reported methods to

prepare phosphorescence paint from seashells. Initially, the usage of phosphor materials was for modifying the colors of output in fireworks. Later, the developments towards device fabrication using these phosphors were attempted by the researchers in 20th century. Earlier in 1940s, the phosphor materials were used in cathode ray tubes majorly for the applications of televisions, computers, monitors and many other display devices and fluorescent lighting. During the last five years, white LEDs have become very important lighting sources and the importance of LED phosphors for white and coloured light generation are major considerations in today's market for lighting purposes [3,4].

1.3 Principle of Phosphors

A material can emit light either through incandescence, where all atoms radiate, or by luminescence, where only a small fraction of atoms, called emission center or luminescence center, emit light. In inorganic phosphors, these homogeneities in the crystal structure are created usually by addition of a trace amount of dopants, impurities called activators. The wavelength emitted center is dependent on the atom itself and on the surrounding crystal structure.

The scintillation process in inorganic materials is due to the electronic band structure found in the crystals. An incoming particle can excite an electron from the valence band to either the conduction band or to the excitation band. This leaves an associated hole behind, in the valence band. Impurities create electronic levels in the forbidden gap. The excitons are loosely bound electron-hole pairs that wander through the crystal lattice until they are captured as a whole by impurity centers. It is rapidly de-excited by emitted scintillation light (fast component). In case of inorganic scintillators, the activator impurities are typically chosen so that the emitted light is in the visible range or near-UV where photomultipliers are effective. The holes associated with electrons in the conduction band are independent from the latter. Those holes and electrons are captured successfully by impurity centers exciting certain metastable impurity states, slowed down by reliance on the low-probability forbidden mechanism.

1.4 Process of Phosphorescence

Phosphorescent materials store and re-emit light because of their unusual property of trapping electrons in a higher state of movement. As light comes in contact with the material, light photons are transferred to the material and give some of their energy to the electrons

within it, causing the electrons to move to a higher energy state around their nucleus. While most photoluminescent materials allow their excited electrons to quickly return to a ground state, phosphorescent materials trap their electrons in a higher energy state for minutes or even hours.

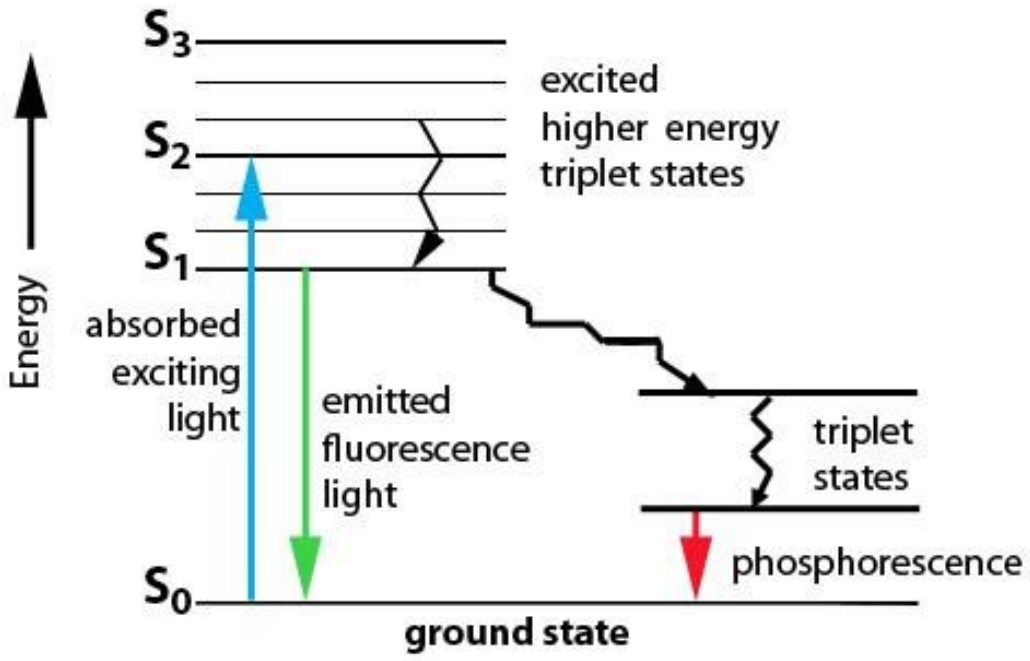

Figure 1.1 Schematic diagram showing the process of Phosphorescence

Phosphors that emit UV, visible or IR light upon UV excitation then show a decline in quantum yield QE. Luminescent materials should be highly crystalline to achieve high light output that is having as few lattice defects and impurities as possible. In addition, the surface area of the crystals has to be minimized, which means that their surface has to be clean and smooth [5,6].

1.5 Application of Phosphors

Phosphor has its enormous application in today's world. It plays a vital role in industries, laboratories and mainly in lighting industry. The remarkable points to be noted in the applications of phosphors are given below:

- Efficient, energy saving and environmentally friendly candidates for general lighting, white light-emitting diodes (WLEDs)
- Great stability, high brightness, long operation time and low power consumption.

- A better replacement for the conventional lighting devices which discharges either heat or gases.
- Robustness, energy efficient, long lifetime and good temporal stability [7].

1.6 Importance of Light Emitting Diodes (LED)

The electromagnetic spectrum consists of a variety of types of electromagnetic waves, each with different wavelengths or frequencies. Only a small portion of the spectrum of wavelengths can be seen by the human eye. This visible portion of the electromagnetic spectrum is called the visible spectrum. White light is the mixture of all the visible wavelengths. The full spectrum that forms white light is listed in the Table given below:

Color	Wavelength
violet	380–450 nm
blue	450–495 nm
green	495–570 nm
yellow	570–590 nm
orange	590–620 nm
red	620–750 nm

Table 1.2 Colors of the Visible Spectrum

The solid-state lighting (SSL) is becoming more common as next generation lighting. Lighting accounts for about one-sixth of residential energy consumption. LED and other forms of SSL consume less energy and are drastically replacing traditional lighting such as incandescent and fluorescent lamps in order to conserve energy. It is necessary to have sufficient light intensity over the full visible light (380 nm-780 nm). A white light LED is suitable to fulfil the requirement and spectra of normal LED and white LED is shown in the Figure 1.3.

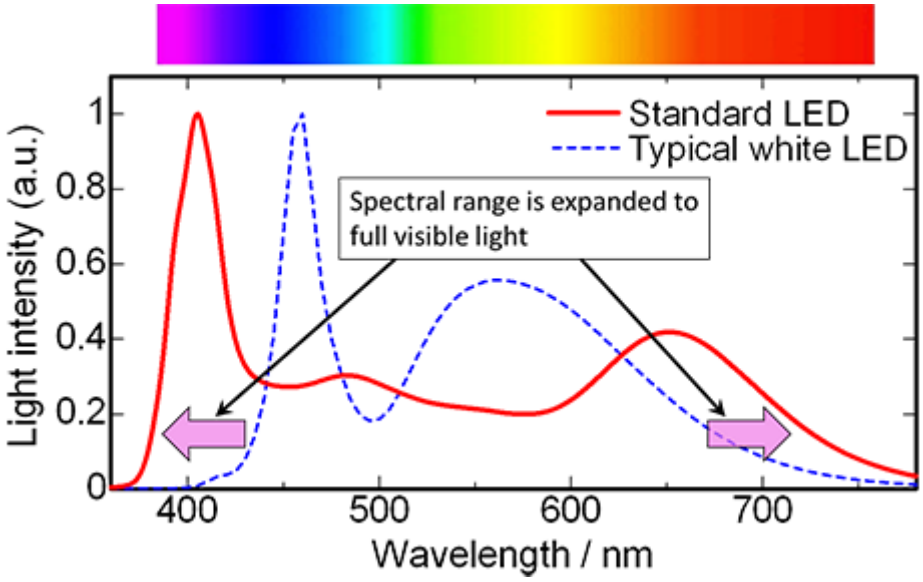

Figure 1.3 Spectra of the developed standard LED and a typical White LED

1.7 Method for generating White light from LED

Light Emitting diodes (LEDs) emit light of a single color in a narrow band of wavelengths, whereas white light is required for a huge range of applications, including LED backlighting for large liquid-crystal displays (LCDs) and general home and office lighting. There are various ways of obtaining white light from LEDs as shown in the Figure 1.4.

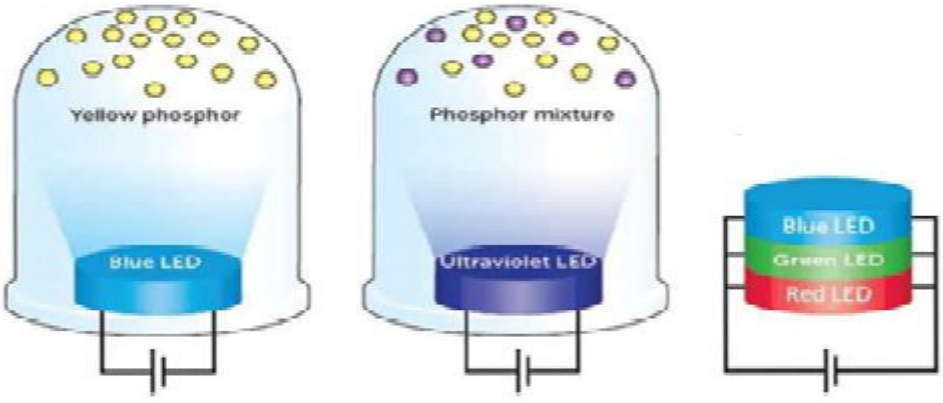

(a) **(b)** **(c)**

Figure 1.4 Three methods for generating white light from LEDs: (a) blue-LED + yellow phosphor (b) UV-LED + RGB phosphors (c) red + green + blue-LEDs

- **Blue LED + Yellow phosphors :** The first commercially available white LED is based on an InGaN chip emitting blue light at a wavelength of 460 nm that is coated with a cerium-doped yttrium aluminium garnet (YAG) phosphor layer that converts some of the

blue light into yellow light. The phosphor layer is sufficiently thin that some blue ligt is transmitted through it, and the combination of blue and yellow produces a cool white light. This is fine for many applications like displays, key rings and cell phones. But the quality of light is probably not good enough for home lighting and for a warmer white light some red light is desirable and it is typically added.

- **UV LED + Red + Green + blue phosphors:** It is a better route to generate warm white light by combining these phosphors together. There are no dangers in using the near-UV LED, since thick phosphor layers would be used so that no near-UV light would be transmitted much, and also in the same way as the phosphor coating on fluorescent tubes and CFLs prevents the transmission of UV light. The major drawback of this method is the intrinsic energy loss from a near-UV photon to a lower-energy visible photon.
- **Red + green + blue phosphors:** Mixing red, green and blue (RGB) LEDs is the obvious way to produce white light. However there are three basic problems with this method. (i) The efficiency of green LEDs is much less than that of red and blue known as "green gap" problem, which limits the overall efficiency of this method. (ii) The efficiencies of red, green and blue LEDs change over time at different rates. If a high quality LED is produced initially, the quality of the white light degrades noticeably over time and this can be corrected by using automatic feedback. (iii) Due to the emission peaks of LEDs are narrower than those of most phosphors, the combination of red, green, and blue LEDs will give a poorer color rendering. This could be minimized by careful choice of LED emission wavelengths for better coverage of the visible spectrum. In particular, using four LEDs, red, yellow, green and blue, can give a good color rendering index [8].

1.8 Available materials for LED application

The major semiconductor materials used to manufacture LEDs are:

- Indium Gallium nitride (InGaN)- blue, green and ultraviolet high-brightness LEDs.
- Aluminium Gallium Phosphate (AlGaInP)- yellow, orange and red high-brightness LEDs.
- Aluminium Gallium Arsenide (AlGaAs) - red and infrared LEDs.

In order to emit light in the visible region of the electromagnetic spectrum, synthesized phosphors have to absorb in the UV to blue spectral range thereby limiting the activators that can be used in the phosphors. The materials are manufactured in such a way to meet the needs of future energy demands using suitable materials with higher efficiency [9].

1.9 Phosphor Degradation

Several mechanisms lead many phosphors to gradually lose efficiency. The degradation of electroluminescent devices depend on frequency of driving current, the luminescence level, and temperature; moisture impairs phosphor lifetime very noticeably as well. The degradation of phosphors are analyzed through various techniques and it occurs due to the following reasons:

- During operation, phosphors can show significant self-heating
- As a consequence of self heating, the conversion efficiency of the phosphors decreases
- Exposure to long-term stress tests at moderate/high temperature levels (in the range of 85°C-145°C) can lead to remarkable degradation of the phosphors [10].

1.10 Shortfall of the present LEDs

On an initial capital cost basis, LEDs are currently more expensive, measured in price per lumen, than more conventional lighting technologies but power saving when looked into the electricity consumption at the end point user side. The additional expense partially stems from the relatively low lumen output, combined with the cost of the drive circuitry and power supplies needed. The shortfall in the present LED system is discussed below.

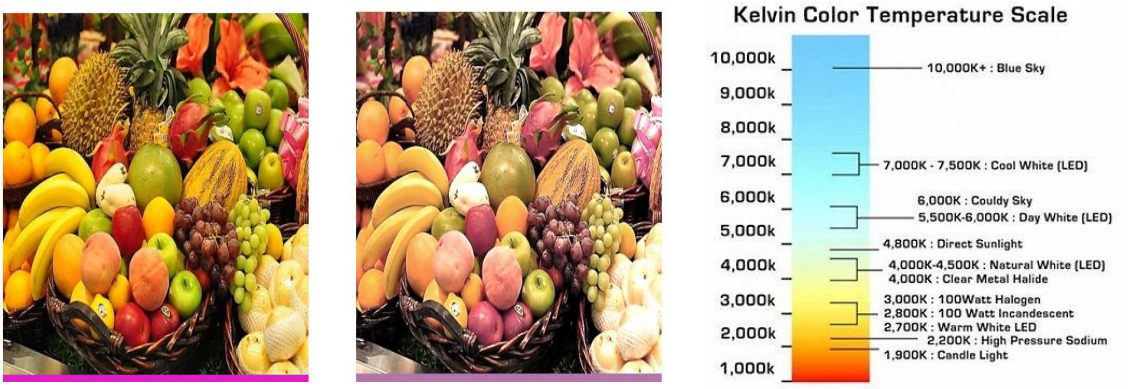

Figure 1.5 Photograph made with incandescent (CRI ~100) and white LED (CRI ~70)

The color rendering in white LEDs are much real when the CRI is nearing 100. The color rendering factor when is greater than 80 Ra in white LEDs they are more close to the Daylight as shown in the color temperature profile in Figure 1.5. The White LED will restore more real color and it is not so in the present commercial LEDs.

1.11 Probable solution for the troubleshoot

There has been evolved many recent research to find the probable solution for the present shortfall of present LEDs, and now the emerging trend is to find a best suited material which could emit tricolor (Red, Green and Blue) towards Day-White light (6000K) with energy efficient means and cost effective solution. This can remain as a probable and better solution for troubleshoot of the present LED system.

1.12 Objective

- To identify a material emitting tricolor (RGB) towards Day-White light.

1.13 Approach

- To prepare Copper sulphide and Tin antimony by co-precipitation method.
- To characterize the Structural, Morphological, Compositional, Thermal and Electronic transition studies.

REVIEW OF LITERATURE

CHAPTER-2

REVIEW OF LITERATURE

11) Schmidt P.C *et al.,* (1992) has studied the electronic band structure, the density of states, and the electronic charge density distribution of K[SnAS], K[SnSb], and Sr [Sn_2As_2] by means of self-consistent density-functional calculations in the local approximation. The valence bands and the conduction bands were separated by a band gap which for one case Sr[Sn_2As_2] was nearly zero. The fully occupied valence bands could be identified as s- and p-like bands of Sn, As and Sb. These results indicated that the alkali and alkaline earth atoms formed a cationic substructure. The Sn and As/Sb atoms formed covalent and negatively charged layer structures. The correlations between the Zintl concept and the calculated band structures were discussed in this work.

12) Vasilev V.P *et al.*,(2003) studied the Sn-Sb system by the electromotive force method and the microstructural, X-ray diffraction, differential thermal calorimetry and microprobe analysis methods. Phenomenological crystal chemical models of the β phase were suggested. The models were based on hexagonal polymorph transformation into a quasi cubic polymorph with a change in crystal symmetry corresponding to a second-order phase transition. The thermodynamic properties of the system were optimized.

13) Lavinia Balan *et al.*,(2005) had prepared the monodispersive SnSb alloy nanoparticles by reduction of $SnCl_2$ and $SbCl_5$ using t-BuONa activated NaOH. The morphology and the structure of the nano-alloy were examined by Transmission Electron Microscopy (TEM), Selected-Area Electron Diffraction (SAED), X-Ray Diffraction (XRD) and X-ray Photoelectron Spectroscopy (XPS). The result showed that very small rhombohedral nanoparticles with an average diameter of 4.7 ± 0.1 nm were produced. This route had provided a promising candidate for studying capacities of nanosized SnSb alloys in electrochemical energy storage devices.

14) H.T. Zhang, G. Wu, X.H. Chen (2006) prepared trigonal and hexagonal CuS (covellite) nanoflakes with controllable size (10-200nm and thickness of 3.6-5nm) which was synthesized through the reaction between copper acetyl acetone and sulphur in oleylamine. Size and shape of the products could be tuned by reaction parameters and reactant concentration. It resulted in a novel procedure for the synthesis of CuS nanoflakes. It was clearly shown that higher reaction temperature and longer reaction time would lead to larger nanoflakes.

15) Keitaro Tezuka , William C. Sheets , Ryoko Kurihara *etal.*,(2007) had extensively studied on the copper sulphide system due to its importance in the fields of mineralogy, geology and corrosion science. Owing to its presence in different varieties of compositions, ranging from copper-rich chalcolite (Cu_2S) to copper-deficient villamaninite (CuS_2) with intermediate compounds in-between, such as covellite (CuS), djurleite ($Cu_{1.95}S$), and anilite ($Cu_{1.75}S$) it could be used for various applications. CuS was prepared by using elemental copper (0.01 mol) and sulphur (0.01 mol) powders ground together. This elemental mixture was transferred with 20ml of distilled water to a 50ml Teflon-lined pressure vessel. The precipitates after reaction were collected by filtration and washed with distilled water several times. X-Ray Diffraction was done to analyze the crystal structure and found to be hexagonal, the XRD pattern of the sample obtained at 60°C for 1 hour reaction time indicated the presence of elemental sulphur and Cu_2O along with those of CuS. The more intense peaks observed for higher temperatures and longer reaction times indicated that the sample contained only copper and sulphur at an average Cu:S atomic ratio 1.01,confirming the stoichiometry. The SEM images showed that the CuS products are obtained at 180°C for 10 hours with the size of 2-3μm in polyhedral phase. A polycrystalline phase of CuS was prepared by the reaction between elemental copper and sulphur at low temperatures (≥60°C) in water.

16) NAN, Zhao-Dong ,WEI, Cheng-Zhen *et.al*., (2008) had investigated the studies on copper sulphide such as Cu_7S_4, $Cu_{1.8}S$, $Cu_{1.81}S$ and Cu_2S, in the wire-like, solid and hollow ball-like shapes congregated from nano-spherical particles and nanoslices. The preparation used was solvothermal method using a mixture of water and ethylene glycol as solvent. $CuSO_4$ and thiourea were used as the starting materials without assistance of any surfactant or template. The results showed that the water content in the solvent affects the morphology of the samples, and the reaction time and temperature affect the crystal structure and morphology. On the basis of the obtained results, the formation processes of different morphologies of copper sulphides were interpreted by the following mechanism: nanoparticles of copper sulphides initially had formed, then the wire-like structures were gradually created, and finally translated to solid and hollow spherical structures under different experimental conditions.

17) Fei Wang *et al.*, (2009) had prepared nano-sized SnSb alloy anodes by reductive co-precipitation method combining with the aging treatment in water bath at 80°C. The microstructure, morphology and electrochemical properties of synthesized SnSb alloy

powders were evaluated by X-Ray Diffraction (XRD), Field-emission Scanning Electron Microscope (FE-SEM) and galvanostatical cycling tests. The result indicated that the cycling performance of SnSb alloy anodes could be improved through reducing particle size. The capacity decline was still apparent in every cycle due to the poor reversible process of high voltage reaction. When the cut-off potential was limited between 0.02 and 0.9 V, the volume and structure changes were alleviated effectively and the excellent cycling performance was obtained within 20 cycles. This paper revealed the effective utility of the nano-sized SnSb alloy anodes for the Li-ion batteries application.

18) Miao Chen,Jing Zhao *et al.*, (2011) successfully fabricated patterned copper sulphide (Cu_XS) microstructures on Si (1 1 1)wafers by a relatively simple solution growth method using copper sulphate, ethylene diamine tetracetate and sodium thiosulphate aqueous solutions as precursors. To obtain high quality copper sulphide thin films, preparative conditions such as concentration, proportion, pH and temperature of the precursor solutions are optimized. Various techniques such as optical microscopy, Atomic Force Microscopy (AFM), X-Ray Diffaction (XRD), Optical absorption and Scanning Electrochemical Microscopy (SECM) were employed to examine the topology and properties of micro-patterned Cu_xS thin films.

19) Yecheng Li, Lei Zhang *et al.*, (2012) investigated the facet effect of copper (I) sulphide nanocrystals based on photochemical properties. CuS nanocrystals were prepared by solvothermal reaction. In a typical procedure of preparing copper sulphide, copper(II) acetyl acetone was mixed with 1-dodecanethiol, toluene and trio-n-octylphosphine. These solutions were placed in stirrer for 10 minutes and the solution was transferred to a sealed Teflon container. The temperature was maintained at 120°C for 12 hours. The products were collected by centrifugation and washed with acetone and ethanol, finally taken for characterizations. Scanning Electron Microscopy (SEM) images showed the morphology and nanostructure with uniform and symmetric 14-facet polyhedron nanocrystals with particle size of approximately 100 nm. Since the reaction rate and formation of nanoparticles were so fast, the particles were obtained with large diversity in size. The chemical composition and crystal structure of the Cu_2S polyhedron nanoparticles had been determined by the EDX and XRD analysis. The EDX spectrum showed an atomic ratio of 2:1 for copper and sulphur. The XRD pattern confirmed the synthesized nanoparticles to be hexagonal. The photoelectrochemical properties of the products were examined under visible light irradiation. This shows that Cu_2S electrode possess p-type character. This work had provided a new strategy for the fabrication of highly efficient visible-light-driven photocatalysts.

20) Joyjit Kundu and Debabrata Pradhan (2013) demonstrated the more synthesis and formation mechanism of copper sulphide (CuS and Cu_2S) by a simple hydrothermal process in the temperature range of 150-250°C. The molar concentration ratio of copper nitrate to sodium thiosulphate precursor, and the reaction temperature played an important role in determining the morphology and composition of the product. At a higher thiosulphate concentration, elemental sulphur precipitated out along with CuS. However, the elemental sulphur got degraded with increasing reaction temperature. The morphology of the as-synthesized product was primarily a sphere-like agglomeration of either nanoparticles or nanoplates. The stability of CuS and the formation of different copper compounds at higher temperature were studied in detail using thermal analysis and X-Ray Diffraction. Agglomerated and dispersed nanoparticles/nanoplates were obtained in the absence and presence of a surfactant in the reaction medium. The pure phase of CuS got completely converted to CuO upon calcining in air at 800°C.The in situ high temperature XRD measurements in a vacuum showed complete conversion of CuS to Cu_2S at 600°C without any intermediate phases. The optical band gap of the as-synthesized CuS nanocrystals is measured as 1.7 eV.

21) Anxiang Wang *et al.*, (2014) had studied the element distribution of Sn-Sb alloy between vapour and liquid phase during vacuum distillation. In this technique, central composite design (CCD) is used to optimize the process parameters influencing the content of Sn in liquid phase and the direct yield of Sn. Distillation temperature, feeding materials and soaking time were the parameters studied.

22) P.Nithyadarseni *et al.*, (2014) had successfully studied the influence of incorporating transition metal impurities such as Fe, Co and Ni on the magnetic and electrical properties of SnSb alloy nanopowders synthesized by reductive co-precipitation method. Structural elucidation of all the samples by X-Ray Diffraction (XRD) confirms hexagonal structure and the morphological observations through Scanning Electron Microscope (SEM) showed a minimal particle size of 20nm for the Co substituted SnSb sample, among all the other impurity incorporated samples. Compositional confirmation of Sn, Sb, Fe,Co and Ni were made using EDAX. The X-Ray photoelectron Spectroscopy (XPS) is used to investigate the surface of SnSb and the change in surface activity due to the addition of transition metal impurities. The magnetic hysteresis studies indicated that SnSb and SnSb:Ni exibited diamagnetic behaviour, while the Fe and Co incorporation resulted in ferromagnetic nature. The conductivity of SnSb:Ni shows a semiconducting nature with negative temperature coefficient of resistance, whereas pure and Co substitution exibited metallic behaviour with

positive temperature coefficient of resistance. The switching of metallic to semiconducting regime was explained in this publication.

23) F. Ghribi, A. Alyamanib, Z. Ben Ayadi et.al., (2015) had studied the behaviour of Copper Sulphide (CuS) nanoparticles synthesised by Hydrothermal route. The Copper Sulphide nanoparticles with the grain dimensions between 10nm to 50 nm were obtained by a simple chemical process in the first step. The reaction of thiourea with different sources of copper in distilled water and adjusting the proportion of reactants were studied. The synthesis of the nanoparticles was made by simple modified hydrothermal route at 90°C for 2 hours followed by annealing at 500°C for 1 hour using different types of Cu-precursors to obtain numerous compositions and structures of copper sulphide Cu_xS (Cu_2S:chalcolite, $Cu_{1.95}S$:djurleite and CuS:covellite) for a fixed copper sulphur mass ratio. The obtained nanopowders are grown onto glass substrates by RF magnetron sputtering technique at room temperature. The optical and structural properties of the films were analysed and the band gap was found to be 2 eV. The obtained layers of thin films were promising candidates for photovoltaic applications particularly as absorber in solar cells.

24) Alok Singh, R. Manivannan, S. Noyel Victoria (2015) had successfully synthesized copper sulphide nanoparticles for solar cell applications by a single step sonochemical method using copper acetate and thiourea as precursors. The effects of sonication time, ultrasonic bath temperature and annealing temperature on particle properties were studied. Synthesized particles were characterized using scanning electron microscope, transmission electron microscope, X-ray diffraction spectrophotometer and UV-visible spectrophotometer. The particles were found to be a mixture of chalcolite, covellite and djurleite.The optical band gap of the particles was in the range of 1.6-2.1 eV. Heat treatment of the particles gave rise to needle shaped particles while a bath temperature of 55°C yielded few nanoplates.

25) M.Nafees, M. Ikram, S. Ali (2015) had worked on the thermal behaviour and decomposition of Copper sulphide nanomaterial synthesized by aqueous sol method wherein Copper sulphate pentahydrate was used as copper ion contributor while sodium thiosulphate pentahydrate (Na_2S2O_3-$5H_2O$) and thiourea (H_2NCSNH_2) were used as sulphur sources. X-Ray diffraction (XRD) revealed the hexagonal phase with crystallite size in the range of 30 nm to 50 nm of the product material. Scanning Electron Microscopy (SEM) confirmed the spherical morphology. Thermal behaviour was revealed by Differential Scanning Calorimeter (DSC) and Thermo Gravimetric Analyzer (TGA). To study the change of phases during crystallization, simultaneous (DSC/TGA) analysis was performed in an open air environment. TGA curve showed that the initial weight loss started in the temperature range 230°C-

320°C,while corresponding DTGA curve merge up and DSC curve showed an exothermic and then endothermic reaction which were mainly due to the removal of sulphur contents and dehydration of water content. This work clearly feature that when heating progresses in air atmosphere, CuS releases the SO_2 and produce Cu_2S and $Cu_{1.8}S$ at 200-300°C which led to an exothermic conversion of copper sulphate and oxysulphate at relatively higher temperature of 400-600°C, subsequently endothermic decomposition of copper sulphate and oxysulphate occured to form CuO. The results were compared with thermal analysis under nitrogen atmosphere and analyzed that there is no mass increment due to the unavailability of O_2 required for thermal oxidation process.

26) P.Nithyadharseni, M.V.Reddy *et al., (*2015) had successfully investigated the Sn-based Intermetallic Alloy Anode Materials for the application of Lithium ion batteries. The intermetallic alloy was synthesized from reductive co-precipitation method from metal chlorides using $NaBH_4$ as reducing agent to improve the electrochemical performance of lithium-ion batteries. Phase composition and particle morphology of the compounds were characterized by x-ray diffraction (XRD), scanning electron microscope (SEM), Raman and Fourier transform infrared spectroscopy (FTIR), Thermal properties of the compounds were characterized by differential scanning calorimetry (DSC). The electrochemical performance of the alloys has been evaluated by cyclic voltammetry which revealed the suitability of this material for lithium ion batteries.

27) Poulomi Roy, Suneel Kumar Srivastava (2015) successfully developed the nanostructured copper sulphides and had demonstrated the synthesis, properties and applications. A series of stoichiometric compositions of copper sulphides from Cu-rich, Cu_2S to Cu-deficient, CuS_2 existed with different crystal structures as well as phases, resulting in different unique properties. The suitable band gap values ranged from 1.2-1.5 eV and unique optoelectronic properties indicated that the material was photocatalytically active and exhibited excellent plasmonic behaviour. The material was also known for promising thermoelectric properties, converting waste heat into electricity through seebeck effect. The nanodimensional form of copper sulphides promoted their use to a more advanced level, tuning their properties with the size of the materials. This paper was mainly based on the compositions, phases and crystal and different synthetic methodologies involved in the fabrication of 0D, 1D, 2D nanostructured copper sulphides. The recent achievements on their use in various applications were also briefly discussed.

28) Peter A.Ajibaje, Nandipha L.Botha (2016) reported the synthesis and structural studies of copper sulphide nanocrystals form copper (II) di thio carbamate single molecule

precursors. The optical studies of the as-prepared copper sulphide nanoparticles were carried out using UV-Visible and photoluminescence spectroscopy. The absorption spectra show absorption band edges at 287nm and considerable blue shift that could be ascribed to the quantum confinement effects as a result of the small crystallite sizes of the nanoparticles. The photoluminescence spectra show emission spectra that are red shifted with respect to the absorption band edges. The structural studies were carried out using powder X-Ray diffraction, transmission electron microscopy, scanning electron microscopy, energy dispersive X-ray spectroscopy and atomic force microscopy. The XRD pattern reveals the formation of hexagonal structure of covellite CuS with estimated crystallite sizes of 17.3-18.6 nm. The TEM images showed particles with almost spherical or rod shapes with average crystallite sizes of 3-9.8 nm. SEM images showed morphology with ball-like microsphere on the surfaces and EDS spectra confirmed the presence of CuS nanoparticles

29) Sana Riyaz, Azra Parveen, Ameer Azam (2016) had demonstrated the synthesis of CuS nanoparticles using sol-gel route with the presence of distilled water at 100°C for 3 hours.X-Ray Diffraction (XRD),Energy Dispersive X-Ray spectrum (EDS),and Scanning Electron Microscope(SEM) techniques were employed to study the microstructural properties of the prepared sample. Crystallite size was calculated as 17.73 nm using Debye-Scherrer formula. The EDS spectrum showed a clear peak of Cu and S elements. SEM images shows the morphology of the CuS nanostructures. Optical analyses were done by UV-Visible and Fourier Transform Infra-Red Spectroscopy (FTIR) techniques. The band gap was calculated by Tauc relation and came out to be 2.89 eV.

30) N.Ali, A. Hussain, R. Ahmed *et al*., (2016) has successfully found a new low price thin film modules of Copper antimony tin Sulphide (CATS) for solar cell applications. CATS thin films were deposited on soda lime glass by thermal evaporation technique followed by a rapid thermal annealing in an argon atmosphere. Structural analysis was done by X-Ray Diffraction (XRD) and the results revealed that the annealed samples were poly-crystalline and their crystallinity was improved with increasing annealing temperature. The constituent elements and their corresponding chemical studies were identified using X-ray photoelectron spectroscopy. The obtained optical band gap of 1.4 eV was found which showed that it was a highly efficient thin film material for sola cell technology. Furthermore, observed good optical absorbance and low transmittance for the annealed CATS thin fims in the visible region of light spectrum assured the aptness of the CATS thin films for solar cell applications.

31) D.Lakshmi *et al.*, (2017) has successfully studied the performance of SnSb: Ce, Co alloy as anode for lithim-ion batteries. The synthesis was carried out by simple co-precipitation method using metal chlorides as starting materials. The structure of the SnSb doped with Ce, Co was studied. Stoichiometric amounts of metal chlorides of tin and antimony and tri-sodium citrate were dissolved in distilled water, followed by the reducing agents $NaBH_4$ and NaOH. Vigorous stirring of mixture resulted in SnSb precipitates in the mixture solution. The powders was tested for structural analysis using X-Ray Diffraction(XRD).The XRD pattern of pristine SnSb illustrates a good crystallinity and pure phase of the alloy. All intense peaks were well indexed to the rhombohedral structure. The particle size for SnSb particle was 20nm. Further studies on Ce and Co co-doped tin-antimony anode were also analyzed for the application in Li-ion batteries.

MATERIALS AND METHODS

CHAPTER III

MATERIALS AND METHODS

3.1 Introduction

This chapter deals with the experimental techniques used in the preparation and characterization of copper sulphide nanoparticles and tin antimony alloy. The effect of pulverization of CuS: SnSb nanoparticles have also been studied. The method adopted for the synthesis is co-precipitation technique for both the chosen materials. Several experimental techniques are employed to understand the properties of prepared materials. The experimental techniques used are as follows:

- X-ray Diffraction (XRD)
- Fourier Transformation InfraRed Spectroscopy (FTIR)
- Ultraviolet-Visible Spectroscopy (UV-Vis Spectroscopy)
- Scanning Electron Microscope (SEM)
- Energy Dispersive X-ray analysis (EDX)
- Photoluminescence (PL)
- Thermal Gravimetric Analysis (TG-DTA)

3.2 Nano particle synthesis

Nanoparticles can be derived from larger molecules namely Top-down approach or built up from smaller particles namely 'Bottom-Up' approach. The various techniques involved in Bottom up approach for preparing nanoparticles are discussed in the following section.

3.3 Synthesis Techniques

Synthesis of nanoparticles is easily achieved through various techniques available in Wet chemical Process. Wet chemical methods are used for producing nano and ultra dispersed inorganic powders from aqueous and non aqueous solutions. Some of the synthesis techniques under this process are,

- Sol-Gel Process
- Hydrothermal Process
- **Co-Precipitation Process**
- Polyol Process
- Combustion Process

3.4 Co-precipitation method

Co-precipitation (CPT) is carried down by precipitation of substances normally soluble under the conditions employed. In the precipitation method, insoluble compounds are precipitated where in the co-precipitation method soluble compounds are precipitated. The process of Co-precipitation is carried out in the preparation of Copper sulphide.

3.4.1 Advantages of Co-Precipitation

1. Simple and rapid preparation.

2. Easy control of particle size and composition

3. Various possibilities to modify the particle surface state and over all homogeneity.

4. Homogeneous mixing of the reactant precipitates reduces the reaction temperature.

5. Simple direct route for the synthesis of fine metal oxide powders, which are highly reactive in low temperature sintering [24].

3.4.2 Synthesis of Copper sulphide by Co-Precipitation method

Copper sulphide is prepared by a co-precipitation method using water as solvent. $CuSO_4$ and thiourea are used as the starting materials without assistance of any surfactant or template. The results show that the water content in the solvent affects the morphology of the samples, and the reaction time and temperature affect the crystal structure and morphology. On the basis of the obtained results, the formation processes of different morphologies of copper sulphides can be interpreted by the following mechanism: nanoparticles of copper sulphides are initially formed, then the wire-like structures are gradually created, and finally translated to solid and hollow spherical structures under the different experimental conditions[25].

Among all the methods of preparation of Copper sulphide listed in the literature, the synthesis of Copper sulphide can be easily done by the **hybrid co-precipitation method**. This method does not need any sophisticated instruments and can be easily done under normal laboratory conditions.

3.4.3 Raw materials used

1. Copper sulphate
2. Thiourea
3. Ethylene glycol
4. Distilled water

3.5 Experimental details

3.5.1 Preparation of Copper Sulphide

Preparation of Copper sulphide is carried out by the hybrid co-precipitation solvothermal method and the method is given below:

Different mol/litre ratios of Copper sulphate and thiourea are tried and in a typical preparation, 0.015 mol/lit of copper sulphate ($CuSO_4.5H_2O$) and 0.005 mol/lit of thiourea (CH_4N_2S) are successful. These compounds are dissolved in 70 ml of distilled water. Copper sulphate in water is stirred for 5 minutes ensuring homogenized solution. The solution of thiourea is added to the copper sulphate solution drop by drop and stirred for 20 minutes. The mixture of copper sulphate and thiourea is kept in an airtight container and is placed in a mantle heater for the solvothermal process to be carried out. Solvothermal process is ensured when the precipitation of nanoparticles of Copper sulphide occurred. The mantle heater was maintained at 50℃ for 3 hours of reaction time with a flow rate of 1.5℃/min until a black precipitate is formed, then the solution is filtered and copper sulphide is obtained which is subsequently air-cooled to room temperature naturally.

The chemical reaction involved in the formation of copper sulphide is discussed below:

$$CS(NH_2)_2+H_2O \longrightarrow (NH_2)_2CO+H_2O$$

When thiourea complex reacts with water, the reactions proceed with the formation of carboxylamine and hydrogen sulphide.

When thiourea solution is added to Copper sulphate dissolved in H_2S, the reduced hydrogen sulphide reacts with copper sulphate ions and forms Copper sulphide (CuS) and sulphuric acid (H_2SO_4).

$$CuSO_4+H_2S \longrightarrow CuS+ H_2SO_4$$

Therefore the balanced complete chemical equation of the process being carried out is,

$$CuSO_4+ CS(NH_2)_2 \longrightarrow CuS+ H_2SO_4+ (NH_2)_2CO$$

Since hydrated complex ($5H_2O$) of copper sulphate is involved in the compound, the copper sulphate involved in producing CuS is reduced by 35%, only 65% of copper is

evolved during the reaction. The weights of $CuSO_4$ should be taken to compensate the loss due to complex water molecule. The ratios are tried so as to compensate the loss due to water molecule.

3.5.2 Preparation of tin antimony alloy

Tin antimony nanoparticle is prepared by wet chemical reductive co-precipitation technique. The materials involved in preparation of tin antimony nanoparticles are as follows:

- Tin Chloride ($SnCl_2$)
- Antimony Chloride ($SbCl_2$)
- Trisodium Citrate ($C_6H_5Na_3O_7$)
- Sodium Chloride (NaOH)
- Sodium Borohydrate ($NaBH_4$)

Appropriate gram molecular weights of metal chlorides like $SnCl_2$ and $SbCl_3$ and $C_6H_5Na_3O_7$ (tri sodium citrate dissolved in distilled water) are weighed. 40 ml of distilled water is added to the mixture and the solution is stirred well for 30 minutes in a magnetic stirrer. Thus the solution A is obtained. The appropriate gram molecular weights of reducing agent NaOH and precipitating agent $NaBH_4$ is taken and add 100 ml of distilled water. The solution is stirred well for 30 minutes in a magnetic stirrer. Thus the solution B is obtained. The solution B is mixed drop by drop into solution A. The solution is dissolved completely for 45 minutes vigorously along with continuous stirring all the way to ascertain homogeneity. The solution is filtered with Whatman filter paper followed by washing with distilled water, dilute HCl, acetone and again distilled water. Thus the succeeding sample is taken for characterizations.

3.5.3 Preparation of pulverized CuS : SnSb

The as-prepared CuS and SnSb powders are pulverized in equal ratios of 1:1. The pulverization is done for 1000 rotations for the powders to get well mixed with each other. During pulverization of the powders, there are no color changes noted. The samples are subjected for XRD, TG-DTA, FTIR, UV-VIS and Spectrofluorimetry.

3.6 Characterization Techniques

3.6.1 X-Ray Diffraction (XRD)

X-rays are electromagnetic radiation of shorter wavelength of the range 0.01 nm and has its higher energy.

Principle

X-Ray Diffractometer works on the principle of diffraction. Diffraction occurs when light is scattered by a periodic array with long-range order, producing constructive interferences at specific angles. The most commonly used technique is the powder X-Ray Diffraction to elucidate the crystalline nature of materials. The scattering of X-rays from atoms produce a diffraction pattern that contains information about the atomic arrangement in crystal [34].

XRD is effectively used for the structural determination, phase analysis, detection of preferred orientation, and deduction of an order disorder phenomenon and also determination of crystallite size of the powder samples.

Working

When a collimated beam of X-ray, with a wavelength typically ranging from 0.5 to 2Å falls over a crystal, it diffracts in pattern characteristic to its structure. In powder X-ray diffraction, the diffraction pattern is obtained from a powder of the material, rather than an individual crystal.

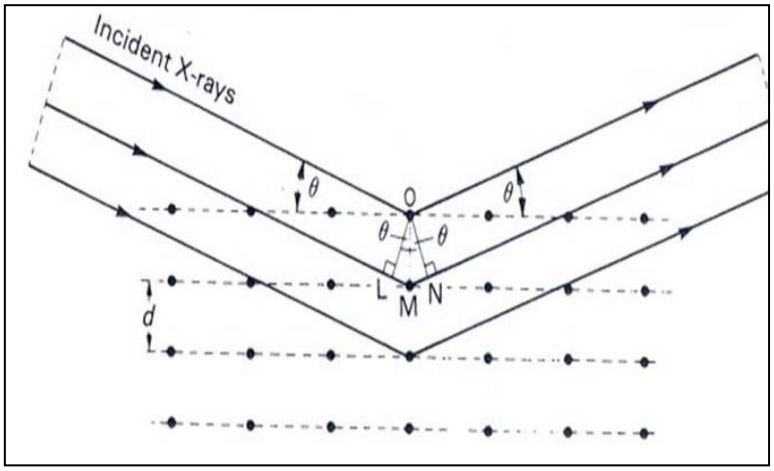

Figure 3.1 :Schematic representation of X-ray production.

Powder diffraction is often easier and more convenient than single crystal diffraction as it does not require individual crystals. The diffraction pattern plots intensity against the angle of the pattern, the peak position depends upon the wavelength Interactions between the incident X-ray beam and the sample produce intense reflected X-rays by constructive interference when conditions satisfy **Bragg's Law.**

$$n\lambda = 2d \sin\theta$$

d is the spacing between atomic planes (Å)

λ is the wavelength of X-rays (Å)

θ is the diffraction angle (degrees)

Scherrer's Formula

If there is no homogeneous strain, the crystallite size (D), can be estimated from the peak width with the Debye-Scherrer's formula,

$$D = k\lambda / \beta \cos\theta$$

λ is the wavelength of X-rays (Å)

β is the full width of half maximum (FWHM) of a diffraction peak (radians)

θ is the diffraction angle (degree)

k is the Scherrer's constant of the order of unity.

Figure 3.2 Powder X-Ray Diffractometer

The above figure shows the image of Powder X-Ray Diffractometer which is used for the analysis of various crystal structures.

The XRD pattern obtained is plotted in graph 2θ along X-axis and the intensity along the Y-axis. The peak position represents the particular crystalline structure of the compound being used for analysis.

3.6.2 Thermal analysis

3.6.2.1 Thermal Gravimetric Analysis (TGA)

Thermal Gravimetric Analysis is carried out in air and in oxygen free nitrogen. It is carried out at different heating rates. It may be method that the result of thermal analysis of a given sample by a given method depends on various aspects. Thermogravimetric deals with the change in the mass of a substance, continuously monitored as a function of temperature or time, when it is heated or cooled at a predominant rate. It provides information on the thermal stability of the sample at different temperatures and pressures of the environmental gases. Chemical changes occur in an oxidative atmosphere providing very useful information regarding characterization of the sample.

3.6.2.2 Differential Thermal Gravimetric Analysis (DTG)

Differential Thermal Gravimetric Analysis measures the temperature, the direction and the magnitude of thermal transitions induced by heating or cooling a material in a controlled way. DTG measures these properties by comparing the temperature of the sample and that of a reference material, which is inert under similar conditions. This temperature difference is measured as a function of time or temperature under a controlled atmosphere and it provides useful information about the transition temperature but also about its thermodynamics and kinetics. Differential Thermal Gravimetric analysis (DTG) determines the weight gain or loss of a phase due to gas absorption or release as a function of temperature under a controlled atmosphere. This technique provides information about the purity of the sample, as well as its water, carbonate and organic content. It is also useful for studying decomposition reactions [35].

Figure 3.3 Instrumentation of TG-DTA

3.6.3 Fourier Transformation Infrared Spectroscopy

- FTIR (Fourier Transform Infra Red) spectrometer obtains a infrared spectra by first collecting an interferogram of a sample signal using an interferometer, then performs a Fourier Transform on the interferogram to obtain the spectrum.

- An interferometer is an instrument that uses the technique of superimposing (interfering) two or more waves, to detect differences between them. The FTIR spectrometer uses a **Michelson interferometer**.

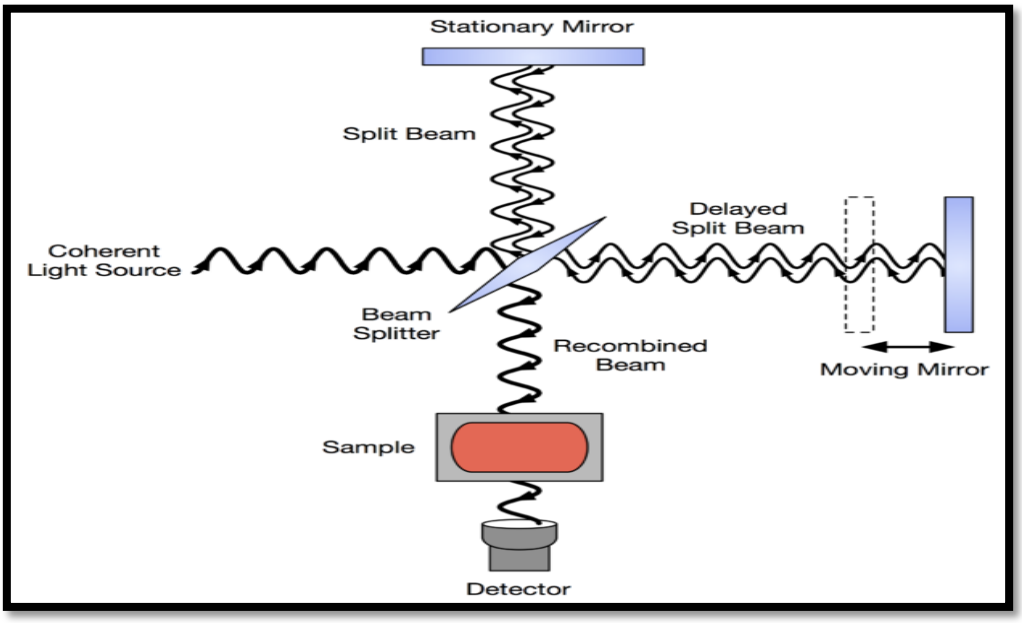

Figure 3.4 Schematic representation of Michelson Interferometer

Working

The heart of the FTIR is a Michelson interferometer (figure 3.3).

- Michelson interferometer which consists of two perpendicularly plane mirrors, one of which can travel in a direction perpendicular to the plane (Figure 4).
- A semi-reflecting film, the beam splitter, bisects the planes of these two mirrors. The beam splitter material has to be chosen according to the region to be examined.
- Materials such as germanium or iron oxide are coated onto an 'infrared-transparent' substrate such as potassium bromide or cesium iodide to produce beam splitters for the mid or near-infrared regions.
- Thin organic films, such as polyethylene terephthalate, are used in the far-infrared region.
- If a collimated beam of monochromatic radiation of wavelength λ (cm) is passed into an ideal beam splitter, 50% of the incident radiation will be reflected to one of the mirrors while 50% will be transmitted to the other mirror.
- The two beams are reflected from these mirrors, returning to the beam splitter where they recombine and interfere. Fifty percent of the beam reflected from the fixed mirror is transmitted through the beam splitter while 50% is reflected back in the direction of the source.
- The beam which emerges from the interferometer at 90◦ to the input beam is called the transmitted beam and this is the beam detected in FTIR spectrometry.[28]

Instrumentation

1) Sources

The sources are always some form of filament which is maintained at red or white heat by an electric current.

The two common sources are

i) **Nernst filament**-It consists of a spindle of rare earth oxides about 1 inch long and 0.1 inch diameter. The Nernst requires to be pre-heated before it conducts electricity, but once red-heat is reached the temperature is maintained by the current.

ii**) Globar filament**-It consists of a rod of carborandum, somewhat thicker and longer than the Nernst.

2) Optical path and Monochromator

- The beam is guided and focussed by mirrors aluminized or silvered on their surfaces. Normally a focus is produced at the point where the sample is to be placed.
- Ordinary lenses and mirrors are suitable as glass absorbs strongly over most of the frequencies used. Any windows which are essential must be made of mineral salt transparent to infra-red radiation which is highly polished in order to reduce scattering to a minimum.
- NaCl which is transparent above 650 cm^{-1} and KBr is transparent above 400 cm^{-1} and are much used.
- A rotatable grating is usually used to disperse the radiation, which have poor resolving power. The prism is usually made of NaCl or KBr.

3) Detector

There are two types of detector which are in common use. One is sensing the heating effect of the radiation, the other depends on the photoconductivity. The greater the effect at a given frequency, the greater is the transmittance of the sample at that frequency.

- **Pyroelectric detectors** such as deuterated triglycine sulphate (DTGS) are commonly used in FT spectrometers. As they are also thermal detectors they are sensitive across the whole IR range, but have the rapid signal response needed in interferometry.
- **Photoconductive detectors** in common use are Indium antimonide (InSb) which can be used above 1400 cm^{-1} and Mercury cadmium telluride (MCT) are used above 700 cm^{-1}.These detectors operate at liquid nitrogen temperature.

4) Sample

The sample is held between plates of polished mineral salt rather than glass. Pure liquids are studied in thickness of about 0.01mm, while solutions are usually 0.1-10 mm thick, depending on the dilution.

- Gas samples at pressure of about 1 atm or greater are usually contained in glass cells either 5 to 10cm long, closed at their ends with rock salt windows.
- Solid samples are more difficult to examine because the particles reflect and scatter the incident radiation and transmittance is always low.

- A technique for handling solids is to grind them very finely with KBr. Under very high pressure this material will flow slightly and the mixture can usually be pressed into a transparent disk. This may then be placed directly in the IR beam in a suitable beam holder.[4]

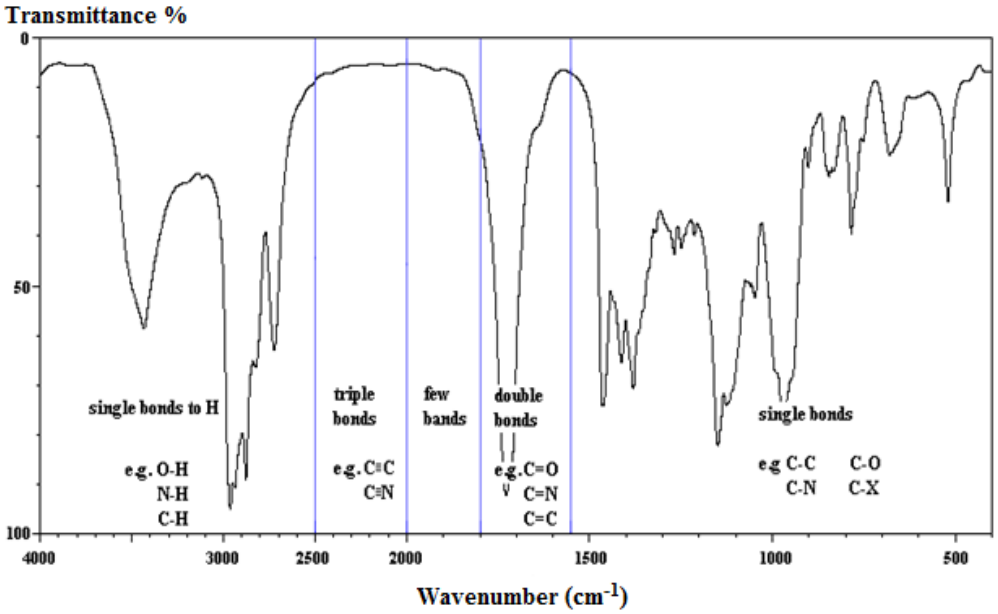

Figure 3.5 Analysis of FTIR results

The graph is plotted against wave number (cm^{-1}) and transmittance (%) for the material to be analysed using FTIR.

Advantages

- Identification of inorganic compounds and organic compounds.
- Identification of components of an unknown mixture.
- Analysis of solids, liquids, and gases [36, 37].

3.6.4 Scanning Electron Microscope (SEM)

Scanning Electron Microscope (SEM) is a type of electron microscope that produces image of a sample by scanning it with a focussed beam of electrons. The Scanning Electron Microscope (SEM) uses a focussed electron beam which is scanned on the surface of the sample to produce high quality images of the surface topography. Scanning Electron Microscope (SEM) essentially offers a very high resolution capabilities and a large depth of focus. It is one of the most widely used techniques used in characterization of nano materials and nano structures.

Instrumentation

The overall design of an electron microscope is similar to that of a light microscope. In the electron microscope, the light is substituted with electrons and the glass lenses are substituted with electromagnetic/electrostatic lenses. The major components of the SEM are discussed below:

- **Electron gun:** Electron gun is the source which is located at the top of the column where free electrons are generated by thermionic emission from a tungsten filament at ~ 2700 K. The filament is inside the Wehnelt which controls the number of electrons leaving the gun. Electrons are primarily accelerated towards an anode that is adjustable from 200 V to 30 kV.
- **Condenser Lenses:** After the beam passes the anode it is influenced by two condenser lenses that cause the beam to converge and pass through a focal point. The condenser lenses are the electromagnetic lenses. The electron beam is essentially focused down to 1000 times its original size. In conjunction with the selected accelerating voltage the condenser lenses are primarily responsible for determining the intensity of the electron beam when it strikes the specimen.

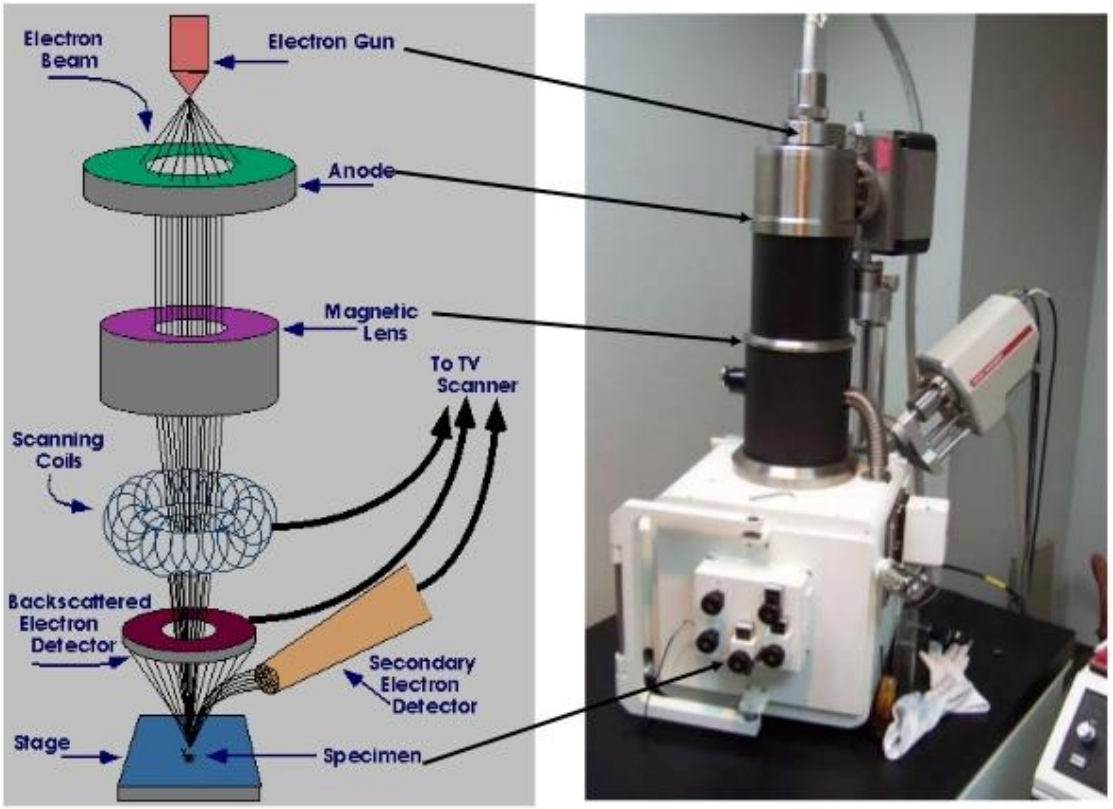

Figure 3.6 Schematic diagram and instrumentation of SEM

- **Apertures:** Depending on the microscope one or more apertures may be found in the electron column. The function of these apertures may be found in the electron column. The function of these apertures is to reduce and exclude extraneous electrons in the lenses. The final lens aperture located below the scanning coils determines the diameter or spot size of the beam at the specimen. Decreasing the spot size will allow for an increase in resolution and depth of field with a loss of brightness.
- **Scanning System:** Images are formed by rastering the electron beam across the specimen using deflection coils inside the objective lens. The stigmator or astigmatism corrector is located in the objective lens and uses a magnetic field in order to reduce aberrations of the electron bem. The electron beam should have a circular cross section when it strikes the specimen however it is usually elliptical thus the stigmator acts to control this problem.
- **Specimen Chamber:** At the lower portion of the column the specimen stage and controls are located. The secondary electrons from the specimen are attracted to the detector by a positive charge.

Scanning Electron Microscope (SEM) provides the morphology of nanostuctured materials and devices, but can also provide detailed information of chemical deposition and distribution [38, 39].

3.6.5 Energy Dispersive X-ray Analysis (EDX)

The Energy-Dispersive X-Ray Spectrometer (EDS) detects X-rays from the sample excited by the highly focused, high-energy primary electron beam penetrating into the sample. The high-energy primary electron beam interacts with the atom of material in this “interaction volume”. Typically several microns in diameter, they generate characteristic x-rays which are fingerprints of the individual atoms encountered. These x-rays can penetrate through the material, allowing them to escape and be obtained from the sample with the aid of the powerful computer and software analysis capabilities. “Standardless” quantitative analyses give an accuracy of 1-2%, while ultimate accuracy can be obtained by spectral comparison to known standards. Detection sensitivities are about 0.1 weight percent. The software also enables one to collect elemental maps of the sample as well as line scans, digitized secondary and backscattered electron images and performs other more sophisticated analyses [39].

3.6.6 Ultra Violet-Visible spectroscopy (UV-Vis Spectroscopy)

Principle

UV spectroscopy is an important tool in analytical chemistry. The other name of UV (Ultra-Violet) spectroscopy is Electronic spectroscopy as it involves the promotion of the electrons from the ground state to the higher energy or excited state. UV spectroscopy is type of absorption spectroscopy in which light of ultra-violet region (200-400 nm) is absorbed by the molecule. The energy of the ultra-violet radiation that are absorbed is equal to the energy difference between the ground state and higher energy states (E=hv). Generally, the most favoured transition is from the highest occupied molecular orbital (HOMO) to lowest unoccupied molecular orbital (LUMO).

Instrumentation

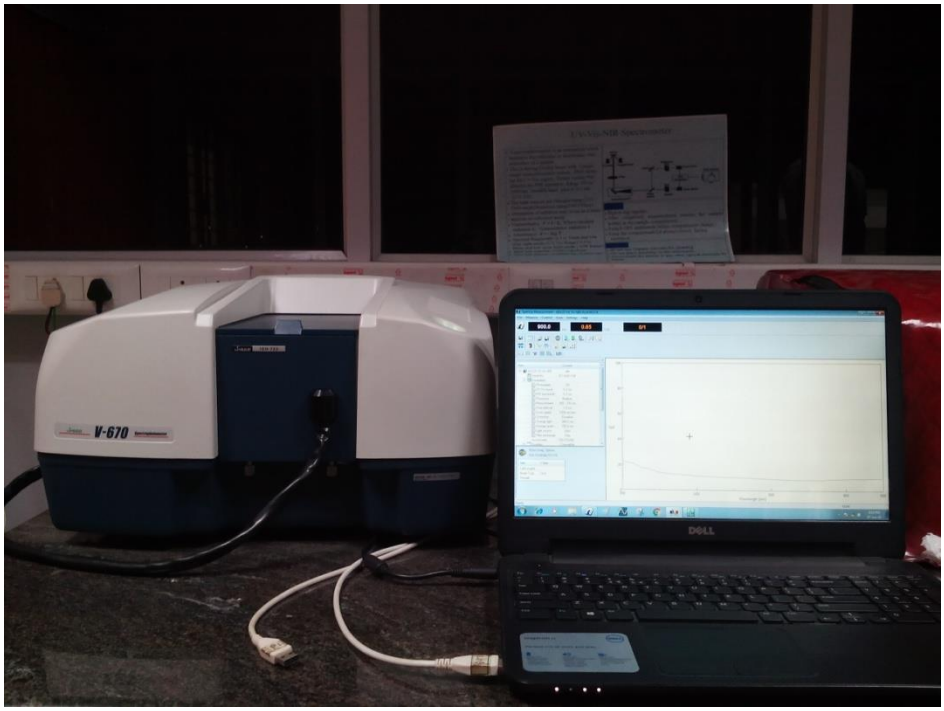

Figure 3.7 Image of UV-Visible Spectrophotometer

Instruments for measuring the absorption of UV or visible radiation are made up of the following components,

- Sources (UV and visible)
- Filter or monochromator
- Sample containers or sample cells
- Detector

1) **Radiation source**-It is important that the power of the radiation source does not change abruptly over its wavelength range.

Various UV radiation sources are as follows,

a. Deuterium lamp

b. Hydrogen lamp

c. Tungsten lamp

d. Xenon discharge lamp

e. Mercury vapour lamp

f. Carbonone lamp

2) Filters or monochromator - All monochromators contain the following components,

• An entrance slit
• A collimating lens
• A dispersing device (a prism or a grating)
• A focusing lens
• An exit slit

Polychromatic radiation (radiation of more than one wavelength) enters the monochromator through the entrance slit. The beam is collimated, and then strikes the dispersing element at an angle. The beam is split into its component wavelengths by the grating or prism. By moving the dispersing element or the exit slit, radiation of only a particular wavelength leaves the monochromator through the exit slit.

3) Sample cells or sample containers

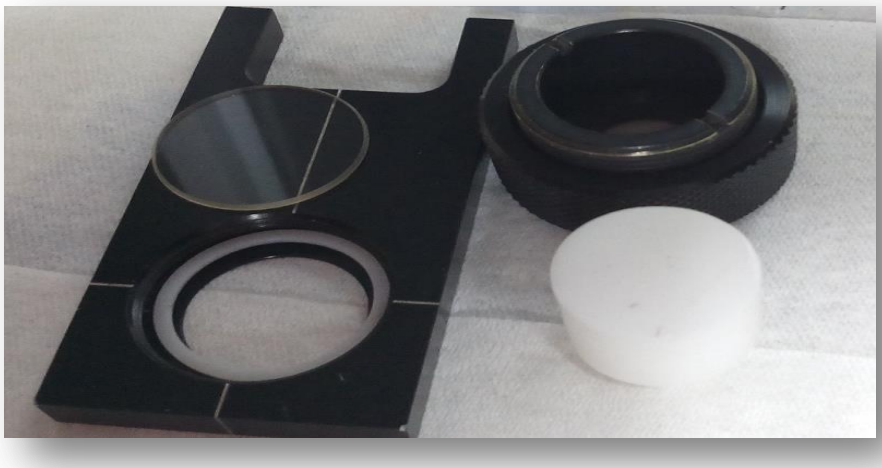

Figure 3.8 Sample cell

Many varieties of sample cells are available for UV region. The choice of sample cell is based on

- The path length, shape, size
- The transmission characteristics at the desired wavelength
- The relative expense

The cell holding the sample should be transparent to the wavelength region to be recorded. Quartz or fused silica cuvettes are required for spectroscopy in the UV region. Silicate glasses can be used for the manufacture of cuvettes for use between 350 and 2000 nm. The thickness of the cell is generally 1 cm, cells may be rectangular in shape or cylindrical with flat ends.

4) Detectors- In order to detect radiation, three types of photosensitive devices are

a) Photovoltaic cells or barrier- layer cell
b) Phototubes or photo emissive tubes
c) Photomultiplier tubes

-Photovoltaic cell is also known as **barrier layer or photonic cell**. When the radiation is incident upon the surface of selenium, electrons are generated at the selenium-silver surface and the electrons are collected by the silver. This accumulation at the silver surface creates an electric voltage difference between the silver surface and the basis of the cell.

-Phototubes are also known as **photo emissive cells**. When radiation is incident upon a cathode, photoelectrons are emitted. These are collected by an anode. Then these are returned via external circuit. And by this process current is amplified and recorded.

-The photomultiplier tube is a commonly used detector in UV spectroscopy. It consists of a photo emissive cathode, several dynodes and an anode.

Photomultipliers are very sensitive to UV and visible radiation. They have fast response times. Intense light damages photomultipliers; they are limited to measure the low power radiation.

Amplifier- The alternating current generated in the photocells is transferred to the amplifier. The amplifier is coupled to a small servo meter. Generally current generated in the photocells is of very low intensity, the main purpose of amplifier is to amplify the signals many times so we can get clear and recordable signals.

Recording devices - Most of the time amplifier is coupled to a pen recorder which is connected to the computer. Computer stores all the data generated and produces the spectrum of the desired compound.

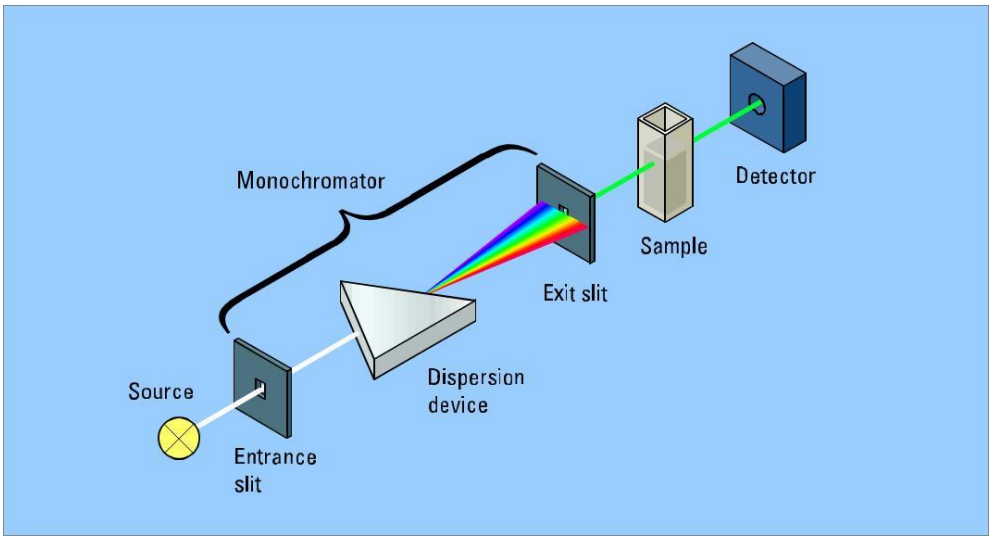

Figure 3.9 Working of UV-Visible Spectrophotometer

Working

- Samples are used in solution and are placed in a small silica cell. Two lamps are used. A hydrogen or deuterium lamp for the UV region and a tungsten halogen lamp for the visible region.
- In this way radiation across the whole range is scanned by the spectrometer. A reference cell containing only solvent is used. Light is passed simultaneously through the sample cell and reference cell.
- The spectrometer compares the light passing through the sample with that passing through the cell.
- The transmitted radiation is deflected and the spectrometer and the spectrometer records the absorption spectrum by scanning the wavelengths of the light passing through the cells radiation across the whole range is monitored simultaneously.
- The principles are the same as for double beam instruments but data on the reference are taken first followed by the sample. In this way single beam instruments can record the spectrum very quickly [36].

3.6.7 Photoluminescence (PL)

Principle

When the external energy supply is by means of the absorption of infrared, visible or ultraviolet light, the emitted light is called **photoluminescence** and this is the process that takes place in any fluorimetric analysis. It is the emission of an absorbed radiant energy in the form of light. The emitted light is almost of wavelength higher than that of the absorbed light.

When a sample is illuminated by a laser, both Raman scattering and photoluminescence (PL) can occur. The latter can be many times stronger than the former and can prevent successful Raman analysis.

- Photoluminescence (PL) comprises both **fluorescence and phosphorescence** processes and originates from an absorption/emission process between different electronic energy levels in the material.
- The amount and type of PL depends on which material is taken for study and which laser wavelength is being used.
- Unwanted fluorescence interference can normally be avoided by choosing an appropriate laser wavelength.
- With most Spectrofluorimeter, it is possible to record both excitation and emission spectra. An emission spectrum is the wavelength distribution of an emission measured at a single constant excitation wavelength. Conversely, an excitation spectrum is the dependence of emission intensity, measured at a single emission wavelength, upon scanning the excitation wavelength. Such spectra can be presented on either a wavelength scale or a wavenumber scale. Light of a given energy can be described in terms of its wavelength λ, frequency ν, or wavenumber. The usual units for wavelength are nanometers, and wavenumbers are given in units of cm^{-1}. For an ideal instrument, the directly recorded emission spectra would represent the photon emission rate or power emitted at each wavelength, over a wavelength interval.
- The process of Photoluminescence can be explained by the Jablonski diagram, which is very much essential in all the atomic and molecular concepts.

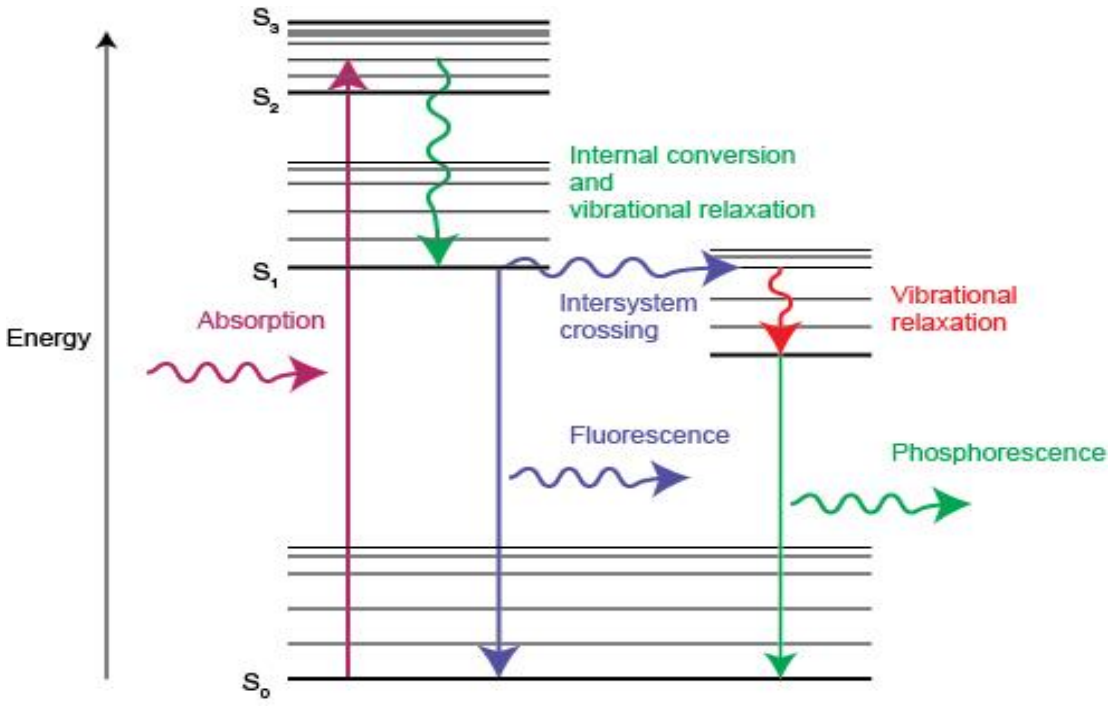

Figure 3.10 Jablonski diagram

The energy differences between vibrational states is about the same for both ground and excited states, the absorption, or excitation spectrum, and the fluorescence spectrum for a compound often appear as approximate mirror images of one another with overlap occurring near the origin transition (0 vibrational level of E_1 to 0 vibrational level of E_0). There are many exceptions to this mirror-image rule, particularly when the excited and ground states have different molecular geometries or when different fluorescence bands originate from different parts of the molecule.

Time periods between absorption and emission may vary ranging from short femto second-regime for emission involving free-carrier plasma in inorganic semiconductors up to milliseconds for phosphorescent processes in molecular systems and under special circumstances delay of emission may even span to minutes or hours.

Observation of photoluminescence at a certain energy can be viewed as indication that excitation populated an excited state associated with this transition energy. While this is generally true in atoms and similar systems, correlations and other more complex phenomena also act as sources for photoluminescence in many-body systems such as semiconductors [40].

RESULTS AND DISCUSSION

CHAPTER IV

RESULTS AND DISCUSSION

4.1 Introduction

This chapter deals with the analysis on the impact of CuS when pulverized with Sn_2Sb_3 alloy. The structural, morphological, thermal and electronic transition studies of the prepared samples are discussed in this chapter.

4.2 Structural Characterization

4.2.1 X-Ray Diffraction Analysis (XRD)

The structural analysis of CuS, Sn_2Sb_3 and pulverized Sn_2Sb_3 : CuS are investigated by X-Ray Diffraction technique. Figure 4.1 shows the X-ray diffractogram of Sn_2Sb_3 prepared by reductive co-precipitation method. The peak positions are observed at 28˚, 40°, 42°, 51°, 59°, 66° and 68° and the corresponding miller planes are (101), (012), (110), (003), (202), (113), (211). All the intense peaks are well indexed to the rhombohedral structure (space group, R-3m). The results are compared to the JCPDS Card No. 33-0118, and there are no evident signals of impurity detected. The intense peak positions and the assignment of miller planes are shown in Table 4.1. Similarly, Copper sulphide (CuS) samples are characterized by XRD. The XRD pattern of as-prepared CuS is shown in Figure 4.2. The XRD peaks of CuS are observed at 21°, 23°, 27°, 29°, 31°, 48°, 52°, 58° and 59° and the corresponding miller planes are (100), (101), (003), (103), (111), (113), (203), (210), (211). The index of assignment for CuS is shown in Table 4.2. It is confirmed through assignment that the structure of CuS is purely hexagonal with a= 4.182Å and c = 8.162Å. The c/a ratio is nearly 2 indicating that the formed compound as a mildly distorted cubic superlattice thus could be more prospective towards an intercalation compound. CuS is annealed at 500°C to find whether thermal dependent phase transition is probable in the sample which is essential to identify the limit of operation of these samples when used in applications like Lithium batteries. The changes are drastic at 500°C as indicated in Figure 4.3 where a normalized diffractograms of CuS as-prepared and CuS annealed samples are given. (Baseline correction has been made for easy comparison in the raw data of both X ray Diffractograms). The assignment of all the reflection in the CuS as-prepared sample are made using the formula for hexagonal crystal structure

$$\frac{1}{d^2} = \frac{4}{3}\left\{\left[\frac{h^2 + hk + l^2}{a^2}\right] + \frac{l^2}{c^2}\right\}$$

The assignments for the as-prepared sample are given in Table 4.2. The lattice parameter values a and c are listed for both CuS and Sn_2Sb_3 in Table 4.4. The peaks corresponding to the hexagonal structure made for the as-prepared samples cannot be observed in the annealed samples thus indicating that CuS cannot withstand this temperature. For clarification, TG-DTA has also been seen and is in good conformity with this result (which is presented in detail in the next section).

The crystallite sizes of all the samples are calculated using Debye-Scherrer formula as follows:

$$\mathbf{D = 0.9\lambda / \beta\cos\theta}$$

where,

D is the crystallite size (nm),

λ is the wavelength of the radiation (1.5405 Å),

β is the full width at half maximum of the peak (radians),

θ is half of the peak position (radians).

Figure 4.4 shows the XRD pattern of CuS : Sn_2Sb_3 pulverized in the ratio of 1:1 wt%. The X-Ray diffractogram of pulverized CuS : Sn_2Sb_3 shows both the indication of CuS and Sn_2Sb_3. The most prominent and highly intense peak is at 28.75° which corresponds to the plane (101) of Sn_2Sb_3 and also at the same 2θ value lies the peak of (103) plane in CuS. Hence, it is well acceptable that this reflection is due to the reinforcement of both these planes in the pulverized sample which has the highest intensity. And the other peaks are predominantly seen at 41.9°, 47.8°, 52.12° and 59.4˚. The peak positions of CuS: Sn_2Sb_3 in correlation with CuS and Sn_2Sb_3 pattern and their assignment of planes are shown in Table 4.3. On comparing the parent compounds and the pulverized one, it is obvious that two compounds have no reaction forming any new compound as almost all the planes that were observed appears. However, the plane (111) observed in CuS has disappeared in the pulverized sample indicating that some change in the arrangement of atoms is prospective on pulverization.

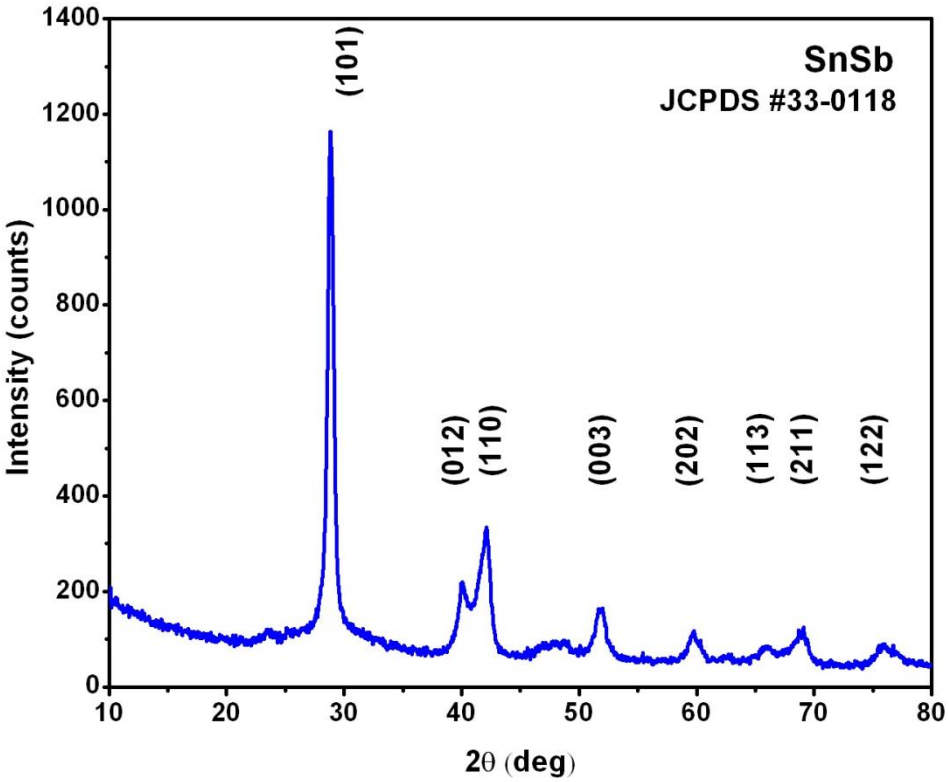

Figure 4.1 XRD pattern of Sn_2Sb_3

Table 4.1 Indexing Planes for Sn_2Sb_3

No. of peaks	2θ (deg)	h	k	l	$1/d^2$ (cal)
1	28.75	1	0	1	0.1037
2	40.00	0	1	2	0.1973
3	42.10	1	1	0	0.2173
4	51.80	0	0	3	0.3220
5	59.60	2	0	2	0.4162
6	66.69	1	1	3	0.4994
7	68.90	2	1	1	0.5398

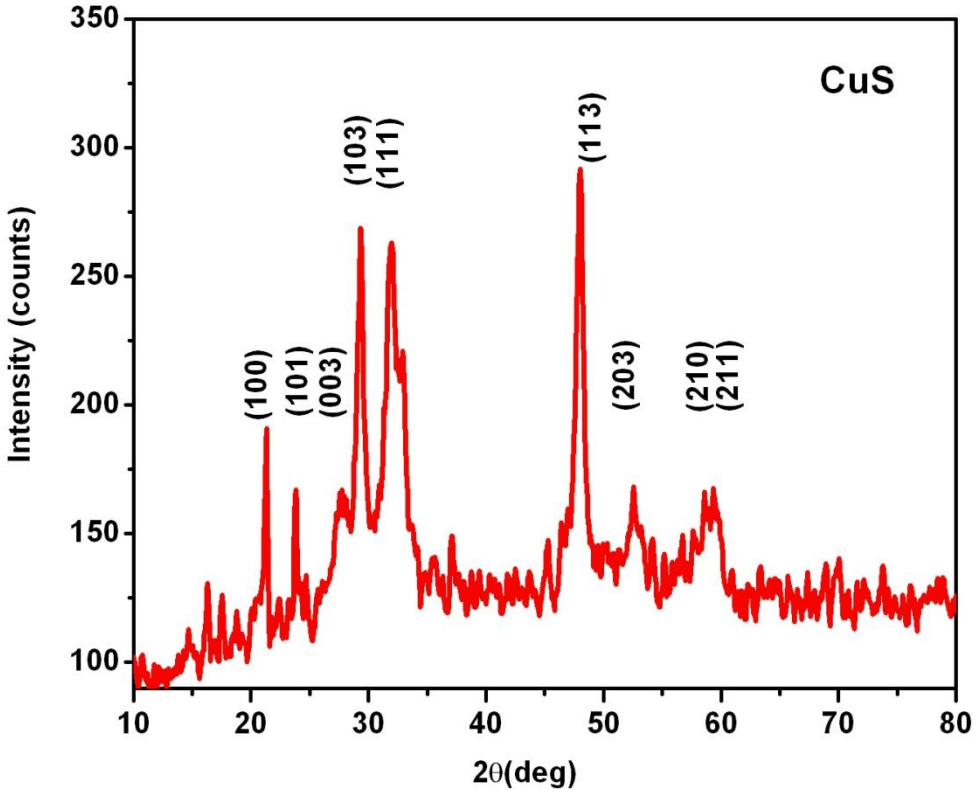

Figure 4.2 X-Ray Diffractogram of CuS

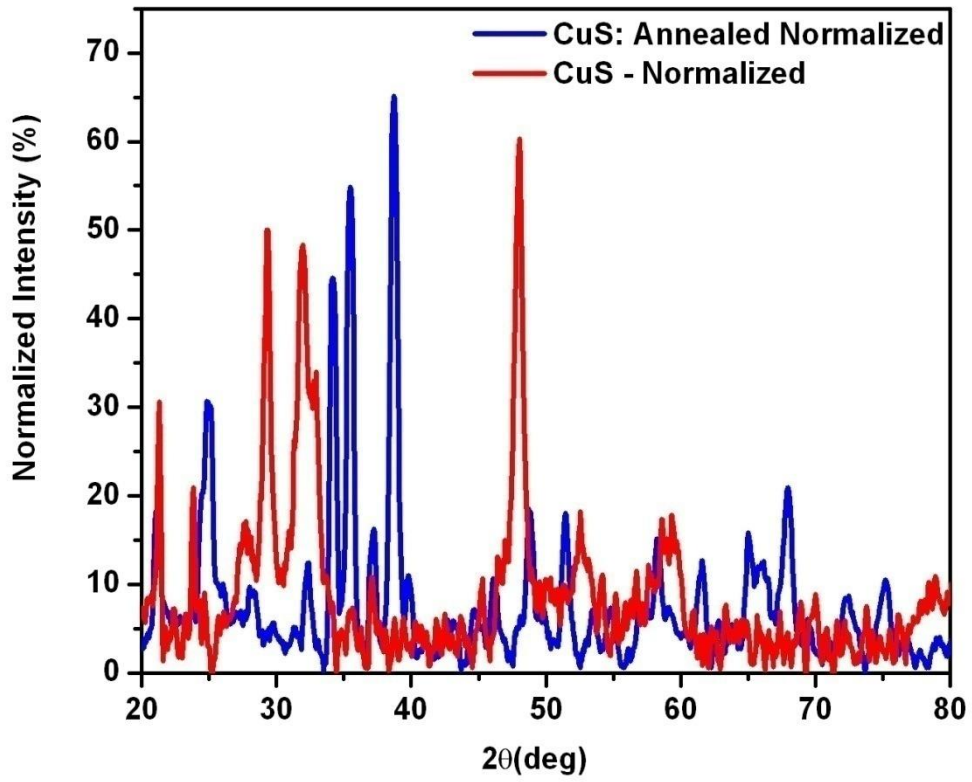

Figure 4.3 Comparison of X-Ray Diffractogram of CuS as prepared and Annealed at 500˚C (Baseline corrected)

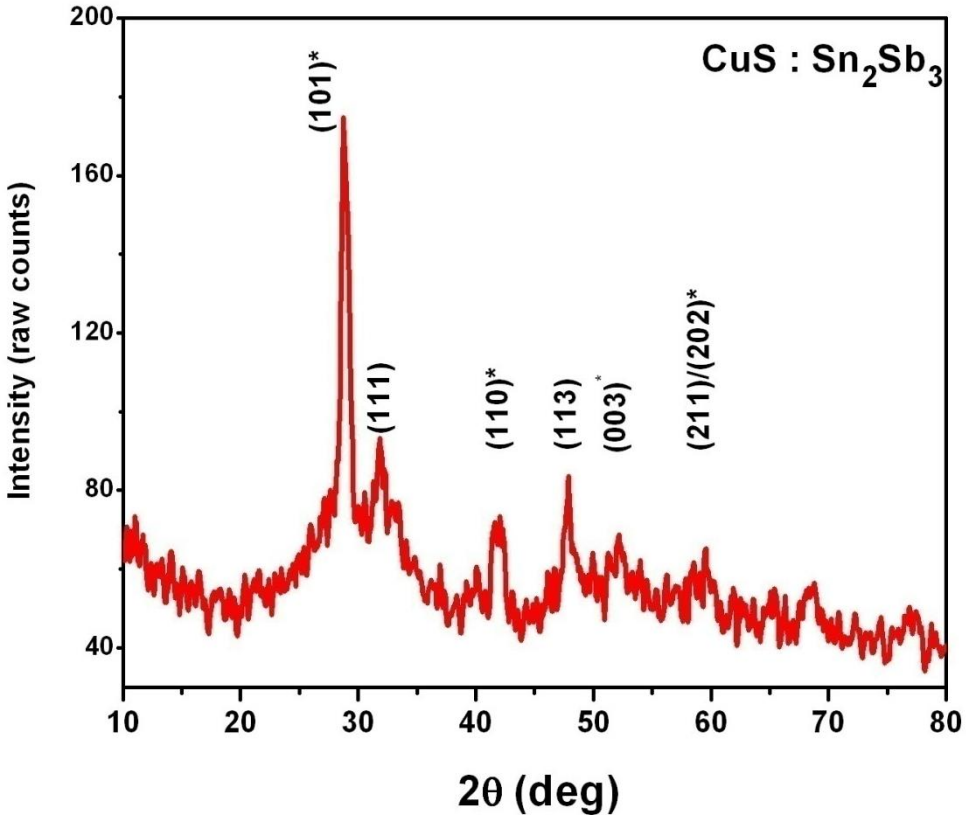

Figure 4.4 X-Ray Diffractogram of pulverized CuS: Sn_2Sb_3 (* - Sn_2Sb_3 peaks)

. Table 4.2. Indexing Planes for CuS

No. of peaks	2θ (deg)	h	k	l	$1/d^2$ (cal)
1.	21.22	1	0	0	0.0572
2.	23.87	1	0	1	0.0721
3.	27.57	0	0	3	0.0958
4.	29.32	1	0	3	0.1080
5.	31.97	1	1	1	0.1279
6.	48.02	1	1	3	0.2792
7.	52.52	2	0	3	0.3302
8.	58.60	2	1	0	0.4039
9.	59.40	2	1	1	0.4140

Table 4.3. Indexing Planes for CuS : Sn_2Sb_3

No. of peaks	2θ (deg)	h	k	l	Peak corresponds to
1.	28.75	1	0	1	Sn_2Sb_3
2.	31.97	1	1	1	CuS
3.	41.90	1	1	0	Sn_2Sb_3
4.	48.02	1	1	3	CuS
5.	52.12	0	0	3	CuS
6.	59.40	2 2	1 0	1 2	CuS Sn_2Sb_3

The crystallite size, lattice parameters and strain calculated for the samples CuS and Sn_2Sb_3 are shown in the Table 4.4.

Table 4.4. Crystallite sizes and lattice parameters of CuS and Sn_2Sb_3 alloy

Sample	Crystallite size (nm)	c(Å)	a(Å)	c/a	$V(Å)^3$	Strain
CuS	17.6	8.162	4.182	1.95	370.86	43.106
Sn_2Sb_3	21.4	5.346	4.325	1.23	86.63	0.0045

In the CuS sample, the maximum peak at 48˚ is used for calculating the crystallite size and in Sn_2Sb_3, the maximum peak at 28° is used for calculating the crystallite size. On comparing the unit cell volume, CuS is nearly 3 times larger than the volume of Sn_2Sb_3. This forms the basis for why the CuS peaks are more predominant in pulverized composition. As the standard c/a value for hexagonal structure is 1.6, the ratio found in Sn_2Sb_3 is less than that (1.2360) and for CuS it is 1.95 as discussed earlier. Further, it is to be noted that when employing the pulverized sample, as the crystal structure of both are hexagonal, the hindrances caused due to the multiphase compositions in intercalation application is expected to be devoid in this case.

4.3 Thermal Characterization

4.3.1 Thermal Gravimetric Analysis (TGA) and Differential Gravimetric Analysis DTG)

Thermal analysis using the instrument SSII TG/DTA 6300 Thermal Analyser s made on all the samples viz., CuS, Sn_2Sb_3 and CuS-Sn_2Sb_3 pulverized. Figure 4.5 (a) shows the thermogravimetric profiles of the CuS at temperature ranging from ambient room temperature to 700°C in nitrogen atmosphere [25]. The TGA curves can be divided into five parts such as Room temperature – 80ºC, 80ºC to 225ºC, 225ºC – 330ºC, 330ºC – 420ºC and >420ºC regions. The first region shows a loss of 5% weight loss which is majorly from 63ºC to 80ºC corresponding to evaporation of moisture. The loss of moisture in this compound can accommodate 15% and the loss of 5% is meagre that ensures that the formed compound is not hygroscopic in nature. It is assured that the compound is stable between 100ºC and 200ºC after the loss of water.

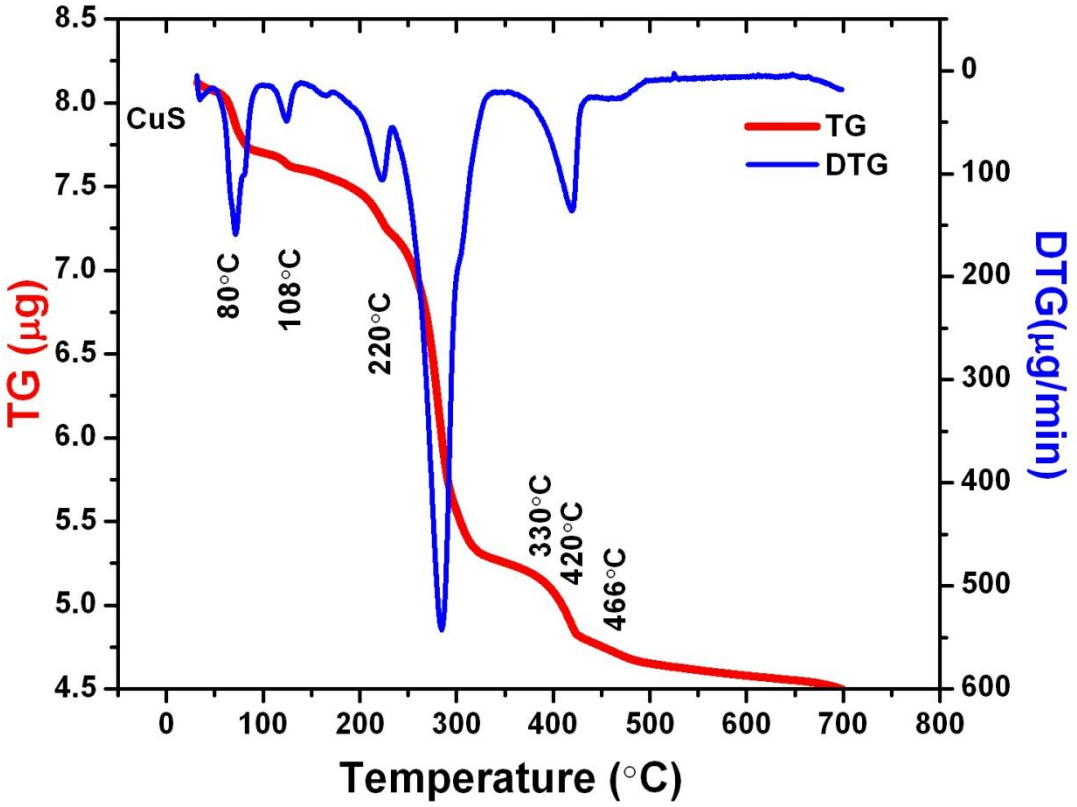

Figure 4.5 (a) TG-DTG for CuS

This is corroborated with the DTG with a peak maximum at 72ºC that is due to the loss of surfacial water and the consecutive mild peak maximum at 125ºC is due to the

moisture trapped by the molecular adsorption in the CuS molecules. A strong inflection is observed at 284ºC which may correspond to the decomposition of CuS molecules. As there is no weight gain in this region, it is assured that the expected Sulphur evolution, resulting in Cu_2S, is not happening in this compound as observed by other workers [41].

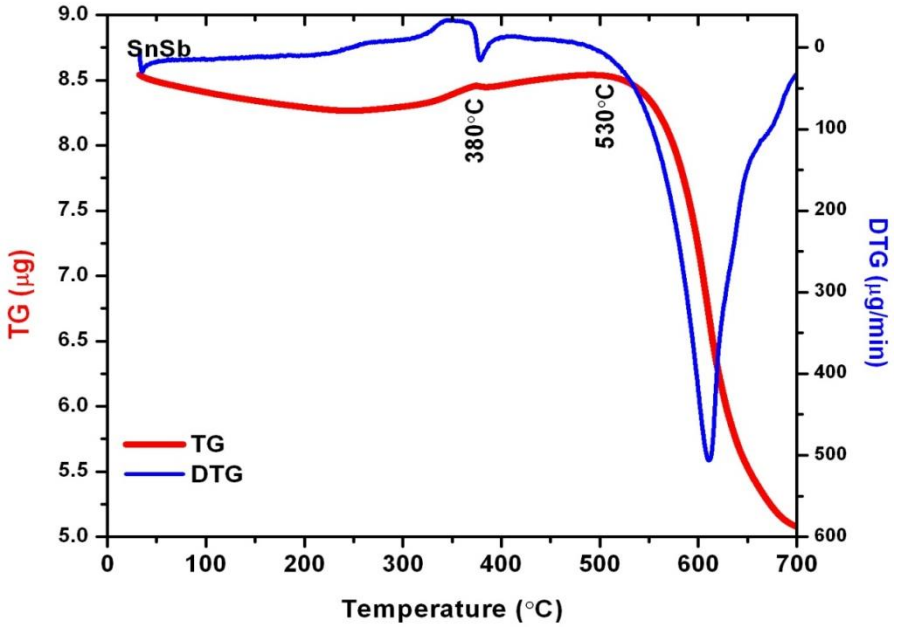

Figure 4.5 (b) TG-DTG of Sn_2Sb_3

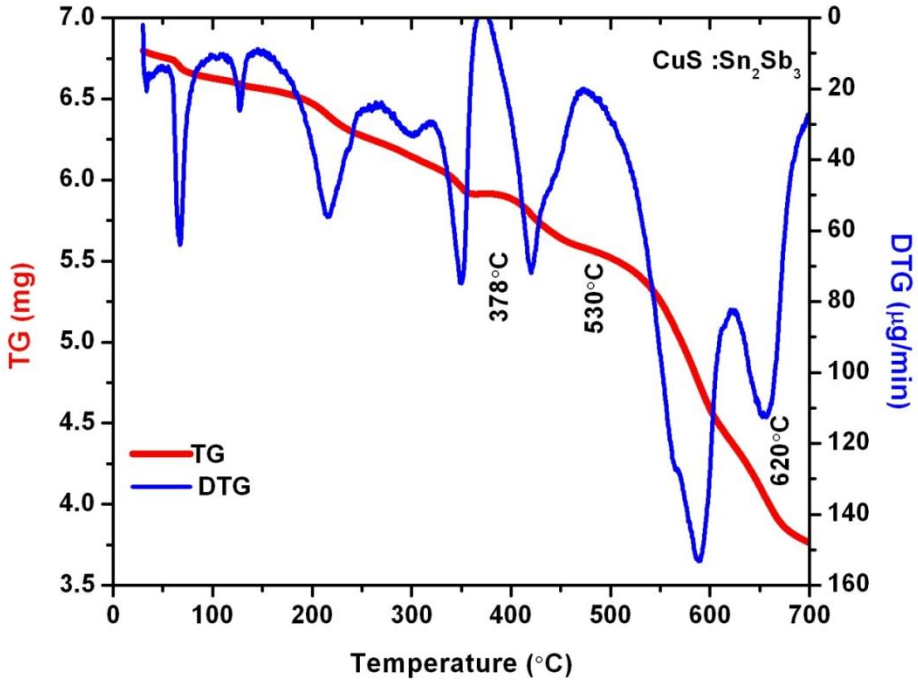

Figure 4.5 (c) TG-DTG of CuS : Sn_2Sb_3

Even after this sulphur evolution region, there is no weight gain observed thus indicating that oxide formation is not much probable. Sublimation occurs after 466ºC.

Figure 4.5 (b) and (c) shows the TG-DTG curves of Sn_2Sb_3 and CuS:Sn_2Sb_3. The pulverized sample of CuS : Sn_2Sb_3 shows the peak similar to the sample Sn_2Sb_3 which is seen at 620°C. The Sn_2Sb_3 sample shows weight loss due to loss of moisture and at 378ºC a slight weight gain is observed which is insufficient for any oxidation but may be a re-crystallizing point for the molecular arrangement. Post re-crystallization, at 530ºC is the decomposition that is complete by 600ºC. Looking at the pulverized sample, no drastic oxidation or formation profile occurs throughout the temperature range of study. Several inflection points of different heights are observed in this thermograph however no drastic oxidation or recrystallization that had appeared as independent compounds has occurred. Thus the pulverization of these two compounds prevents oxidation and adds value over stabilization process of these compounds.

4.4 Morphological Characterization

4.4.1 Scanning Electron Microscope (SEM)

Scanning Electron Microscope is used for the morphological study of CuS and Sn_2Sb_3 nanoparticles. Figure 4.6 shows the SEM images of CuS nanostructures at different magnification, which clearly reveals that CuS nanoparticles are spherical in shape and uniformly distributed [33]. Higher magnification indicates that it is a mixture of spherical particles, flakes and rods. Figure 4.7 shows the SEM image of Sn_2Sb_3 nanoparticles which confirms the presence of very small, uniformly distributed spherical nanoparticles compared to CuS. It also reveals that the image does not show any agglomeration of the Sn_2Sb_3 nanoparticles. The grain size of CuS ranges from 144 nm to 247 nm and similarly the grain size of Sn_2Sb_3 also ranges from 141 nm to 250 nm.

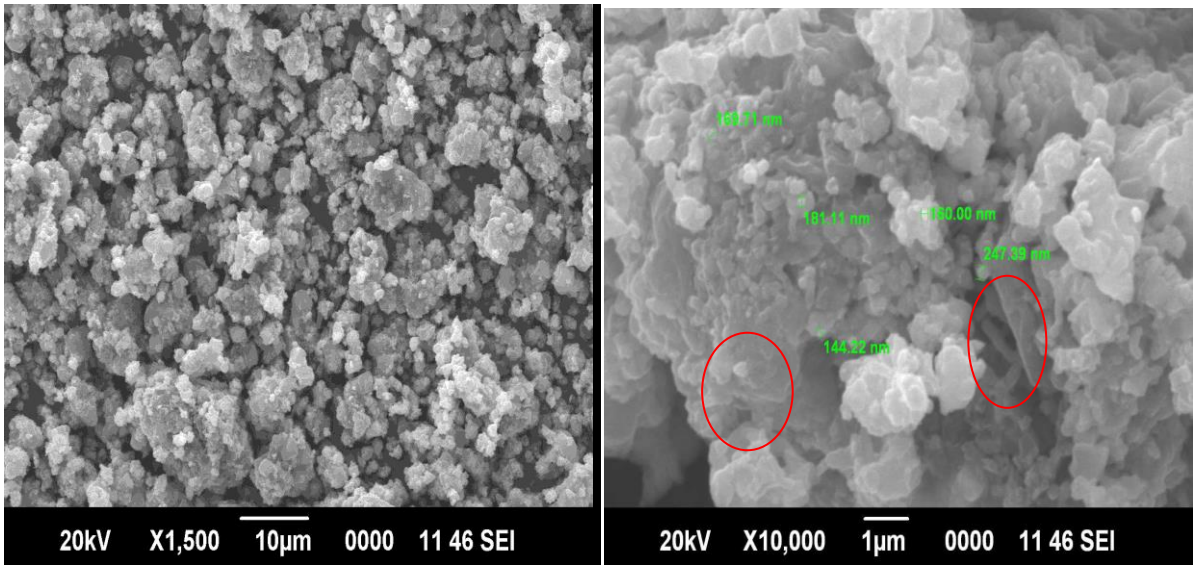

Figure 4.6 SEM images of CuS nanostructures

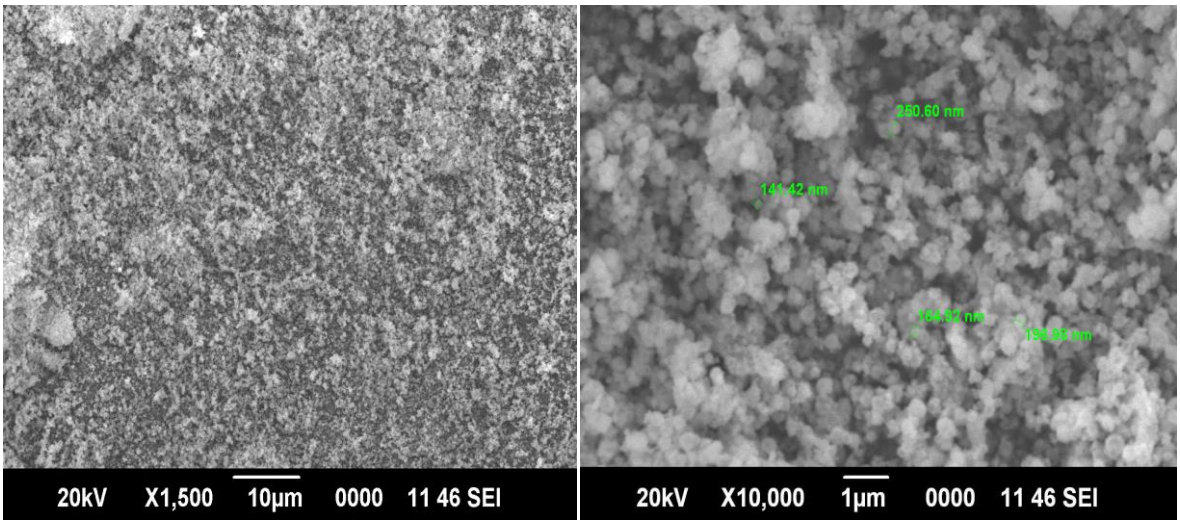

Figure 4.7 SEM images of Sn_2Sb_3 nanoparticles

4.5 Energy Dispersive X-Ray Analysis (EDX)

Compositional analysis of the sample CuS and Sn_2Sb_3 shows the stoichiometric composition of the samples. The EDX spectrum of CuS and Sn_2Sb_3 are shown in the figure 4.8 and 4.9. From the compositional analysis, the molecular formula of the prepared compound obtained as $\mathbf{Cu_{0.75}S_{1.5}}$.The EDS confirms the presence of both copper (Cu) and sulphur (S) in the compound CuS. The molecular formula for the prepared Sn_2Sb_3 is obtained as $\mathbf{Sn_2Sb_3}$. The oxygen present in the EDX is only due to the low vacuum in the chamber of SEM instrument.

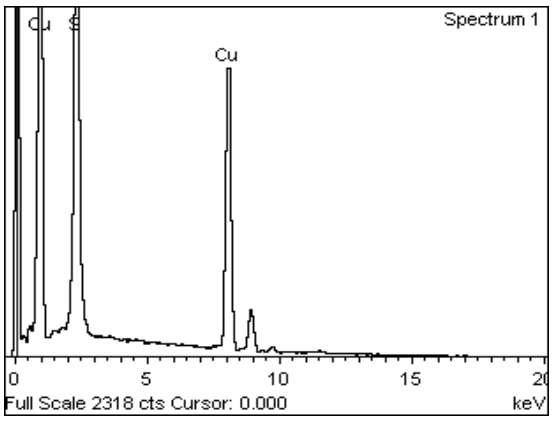

Figure 4.8 EDX spectrum of CuS

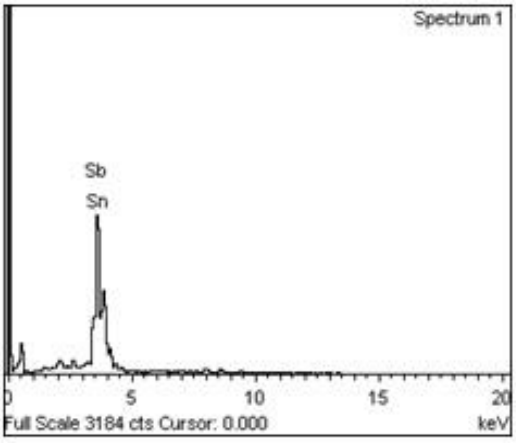

Figure 4.9 EDX Spectrum of Sn_2Sb_3

4.6 Fourier Transformation Infrared Analysis (FTIR)

FTIR spectra of Copper sulphide (CuS), Tin antimony (Sn_2Sb_3) and Copper sulphide with tin antimony pulverized powders obtained by co-precipitation process are recorded at room temperature in the wavelength range of 4000-400 cm^{-1} in the instrument FT/IR-4600 type-A. Figure 4.10 shows the FTIR spectra of CuS. Figure 4.11 shows the FTIR spectra of Sn_2Sb_3. The FTIR spectra of CuS show a broad absorption peak around 3170 cm^{-1} that corresponds to the vibration mode of water absorbed on the surface of the sulphide products. The feature observed at 3757 cm^{-1} and 2361cm^{-1} in all the samples might correspond to artefact of the measurement and hence neglected. The band occurring at 1608 cm^{-1} in CuS, 1590cm^{-1} in Sn_2Sb_3 and 1620cm^{-1} in pulverized sample corresponds to OH bending of moisture. The wavenumber 614cm^{-1} and 1114cm^{-1} corresponds to CuS [42] is observed in both CuS and the pulverized sample, Figure 4.12. In addition, 1899cm^{-1} due to Cu-O bonding [43] is observed in the CuS sample which is not present after pulverization. Thus it is confirmed that there is surfacial oxide present in the CuS sample as no CuO peaks were observed in the XRD also. Moreover, the pulverization of CuS and Sn_2Sb_3 prevents oxidation of CuS as this peak is not observed in the pulverized sample. When looking at the Sn_2Sb_3 spectrum, as there are no peaks at 718, 802 cm-1 which are characteristic of SnO2, it is assured that the samples are devoid of oxides of tin. Similarly, the absence of 551cm^{-1}, 535cm^{-1} and 631cm^{-1} corroborates the absence of oxide of antimony as well.

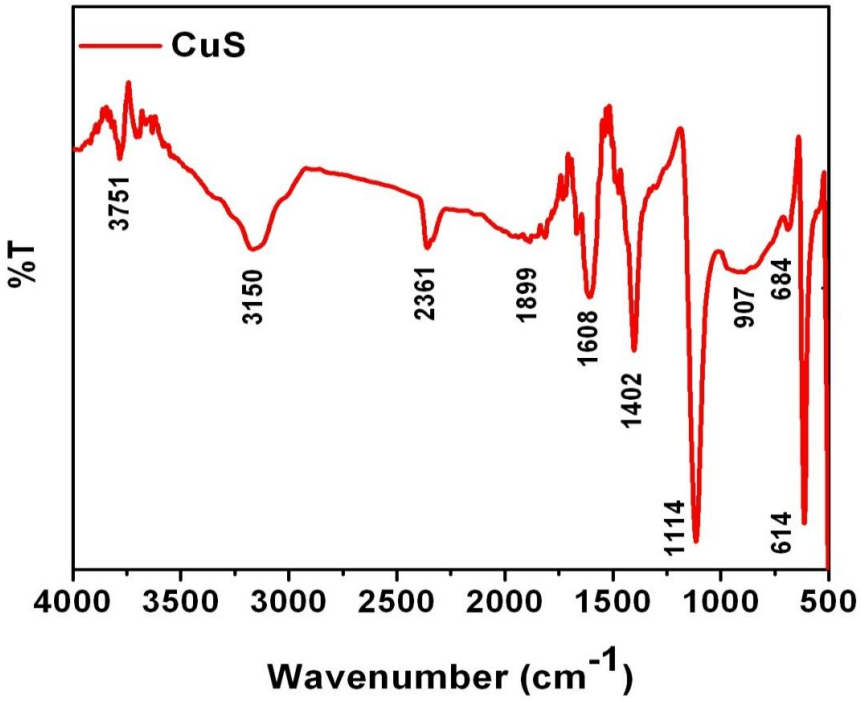

Figure 4.10 FTIR spectra of CuS

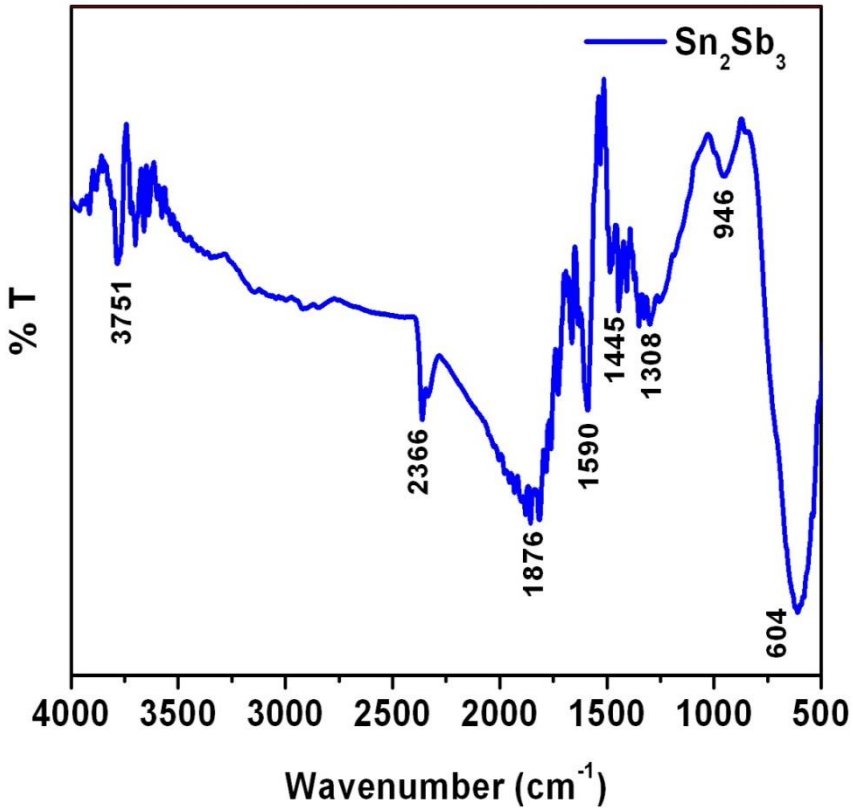

Figure 4.11 FTIR spectra of Sn_2Sb_3

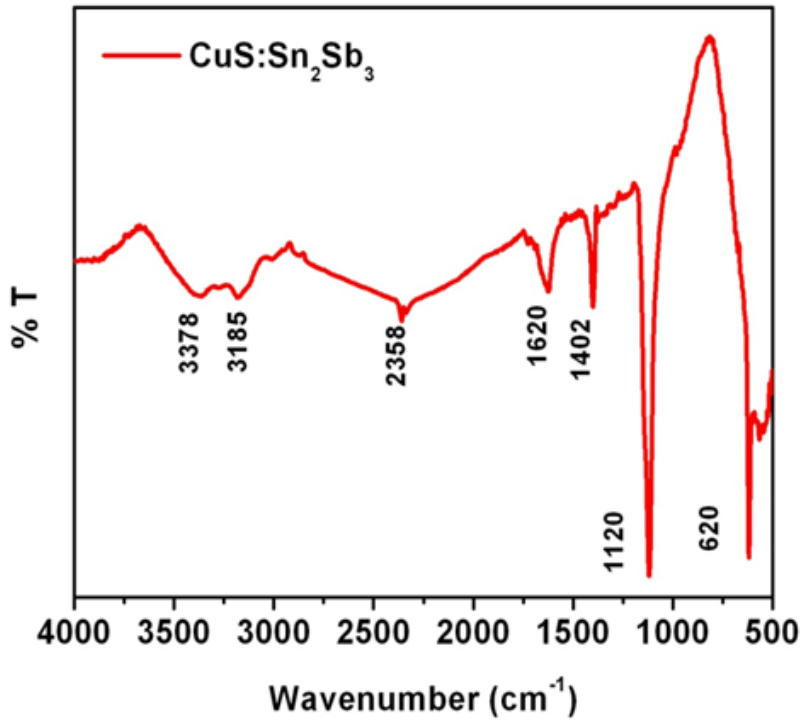

Figure 4.12 FTIR spectra of CuS-Sn_2Sb_3

4.4 Optical Characterization

4.4.1 UV-Visible analysis

UV-Visible spectra recorded for all the samples are discussed in this section. UV-Visible spectra are recorded by the instrument JASCO-V600. Figure 4.13 (a,b,c) shows the absorption spectra of CuS, Sn_2Sb_3 and CuS-Sn_2Sb_3. A weak and broad absorption is seen at the visible region 400-800 nm. However several absorptions are noticed at 207nm, 227nm, 269nm and 367nm.

The UV-Vis spectrum of Sn_2Sb_3 shows major absorptions at 378nm, 423nm, 670nm and 740nm respectively. Figure 4.13 (b) shows the absorption peaks of Sn_2Sb_3 alloy. The absorption peaks of pulverized CuS : Sn_2Sb_3 for 1:1 ratio resembles that of CuS. The absorption peaks are 208nm, 225nm, 270nm, 353nm and 371nm and a fully broad absorption is seen around 400-800nm shown in figure 4.13(c). So it is clear that there is absorption along the visible region and hence this pulverized sample is hopeful to result in tri color emission as expected for the application of white light.

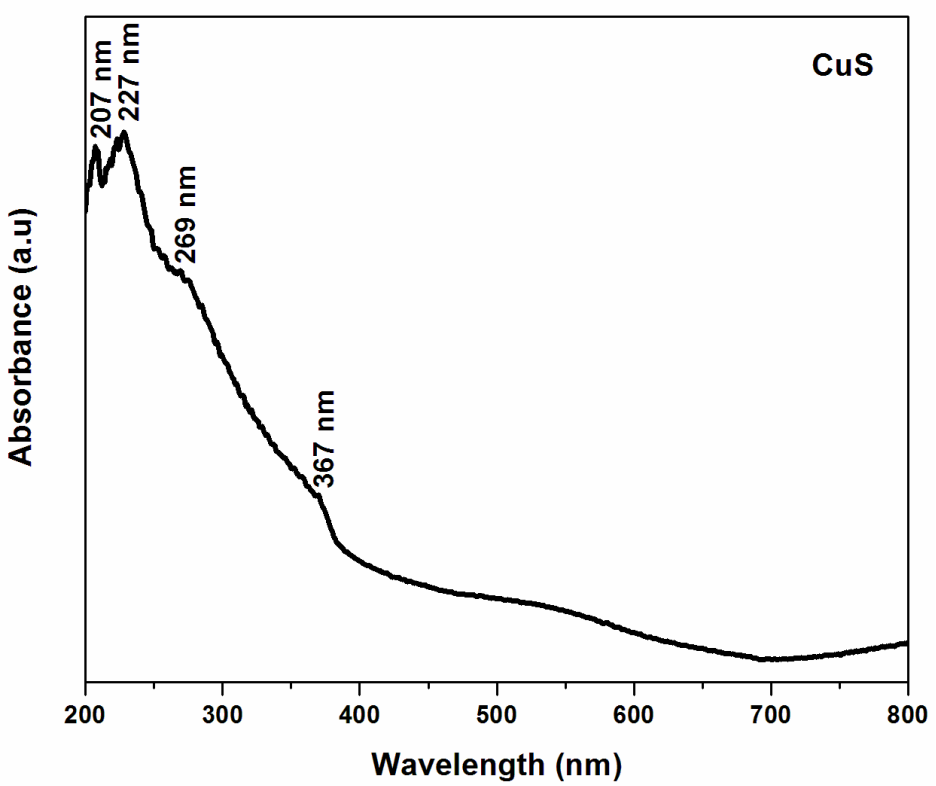

Figure 4.13 (a) UV-Visible spectrum of CuS

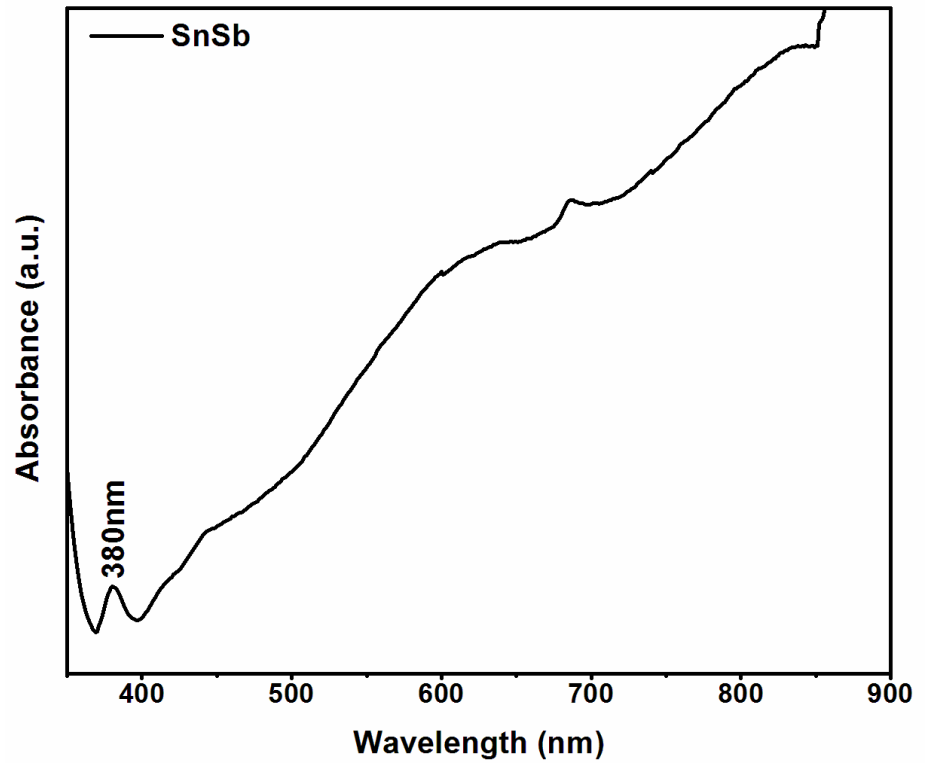

Figure 4.13 (b) UV-Visible spectrum of Sn_2Sb_3

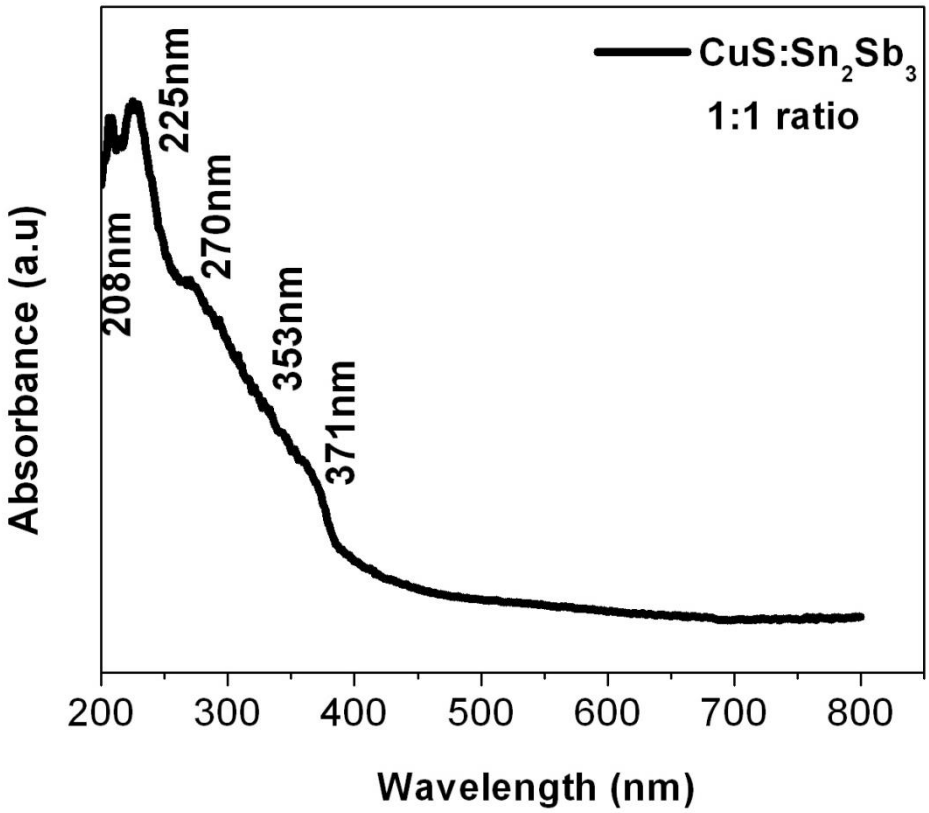

Figure 4.13 (c) UV-Visible spectrum of CuS : Sn_2Sb_3

The energy band gap values of all the samples are calculated by using the Tauc plot. Figure 4.14 (a) shows the Tauc plot of CuS and the energy band gap value is found to be 2.8eV. Figure 4.14 (b) shows the K-M plot of Sn_2Sb_3 and the energy band gap value is equal to 3.5 eV. And the pulverized sample of CuS: Sn_2Sb_3 shows a energy band gap of 2.8 eV which is an intermediate value between the band gap values of CuS and Sn_2Sb_3 shown in figure 4.14 (c).

The emission profiles of all the absorption peaks were checked and the salient excitation was fixed at 345 nm and is presented by the photoluminescence analysis.

4.4.2 Photoluminescence analysis

Figure 4.15 (a) shows the emission spectra of CuS excited at 345nm. The CuS sample exhibited absorption at several wavelengths and the excitation spectrum was fixed for wavelengths along the absorption region 365nm and found the emissions at 345nm (prominent) and 334 nm (feeble). Hence the excitation spectrum is recorded fixing the emission wavelengths as said above. The 345nm peak is majorly populated by 363nm,

390nm, 468nm, 657nm and minor contributions from 374nm. When the excitation is fixed at 629 nm, emission was found at 350nm and 421 nm which is shown in figure 4.15 (b).

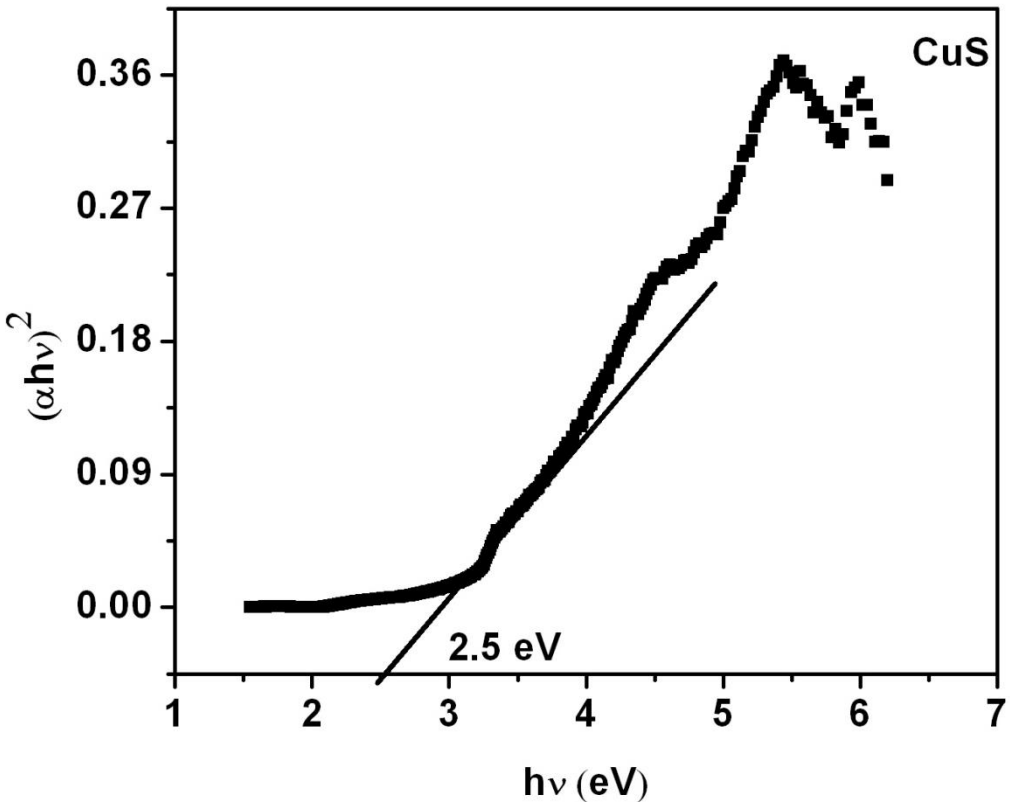

Figure 4.14 (a) Tauc- plot for CuS

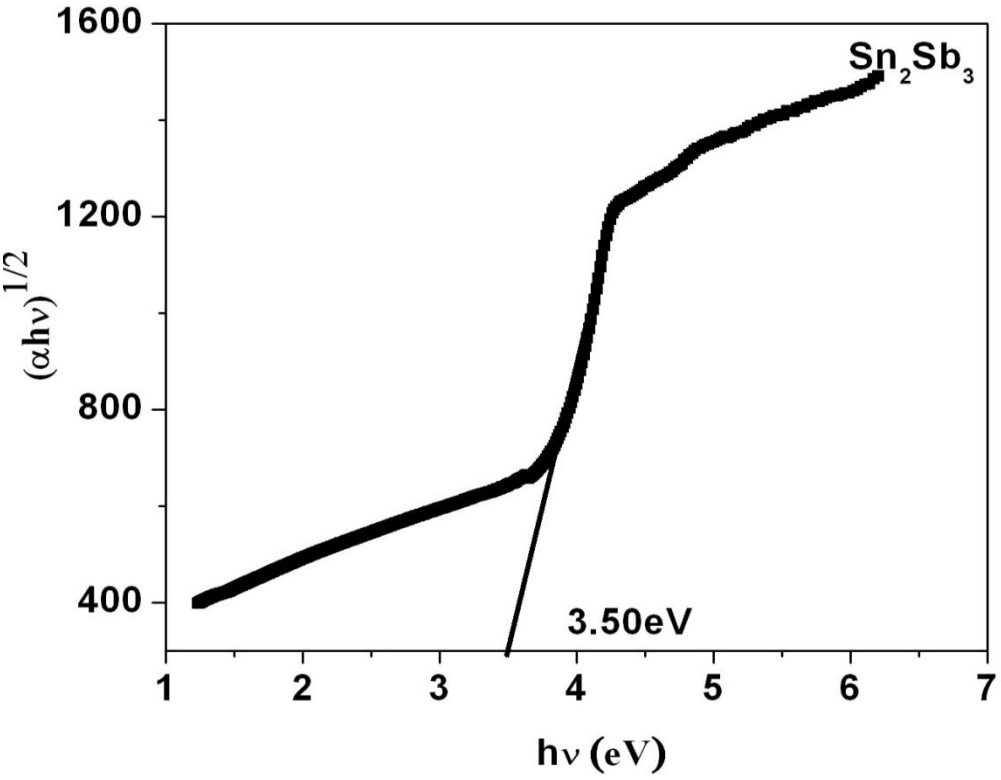

Figure 4.14 (b) Tauc-plot for Sn_2Sb_3

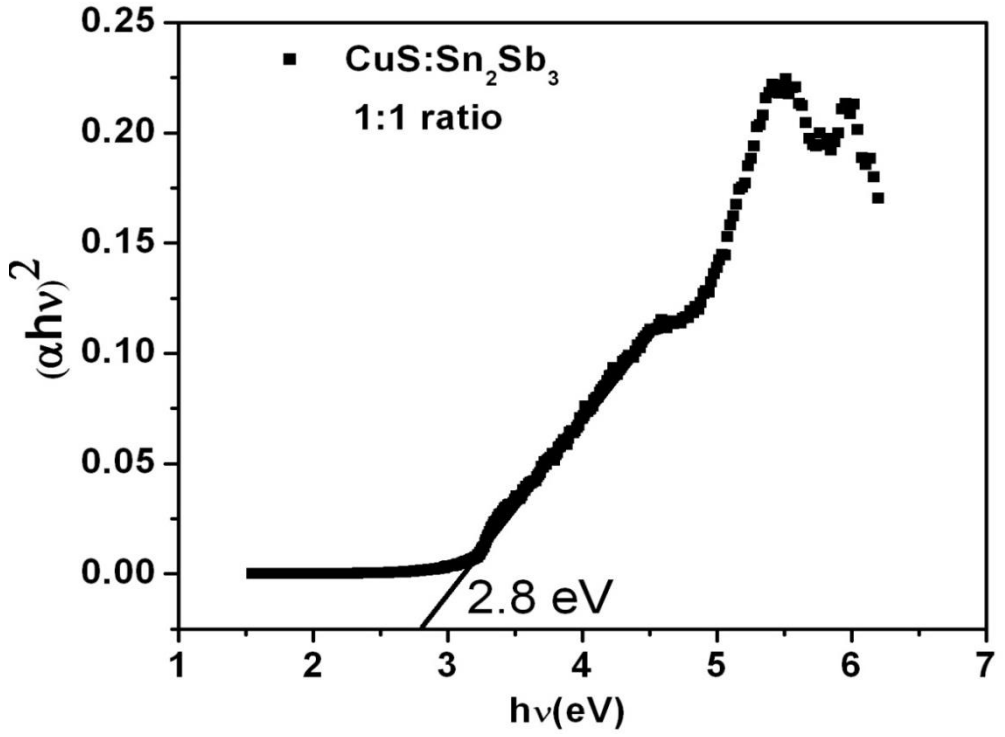

Figure 4.14 (c) Tauc-plot for CuS : Sn_2Sb_3

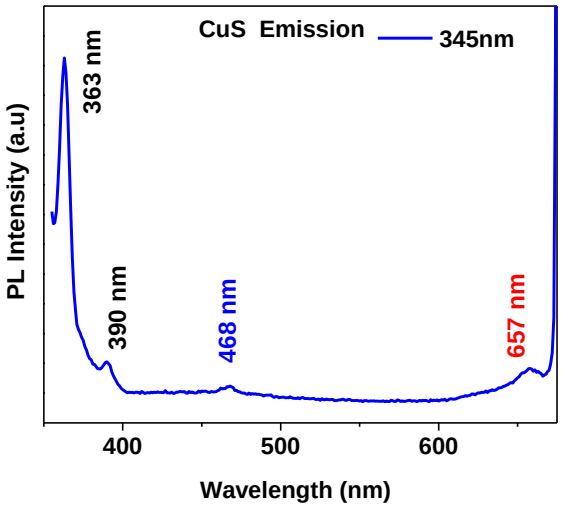

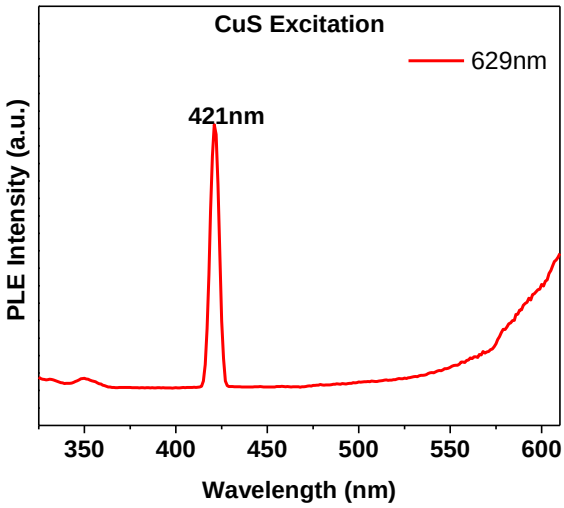

Figure 4.15 (a) Emission Spectrum of CuS **Figure 4.15 (b) Excitation Spectrum of CuS**

Figure 4.16 (a) shows the emission spectrum of Sn_2Sb_3. When excited at 300 nm, emission is being observed at 356 nm, 467 nm and along the range of 712 nm. When excited at 333 nm, emission is observed at 356nm, 388 nm, 465nm and also found emission at 690nm,710 nm and 777 nm. The emission wavelengths are compiled for both the wavelengths 300 nm and 333 nm to avoid the overtones of the spectrum. Figure 4.16 (b) shows the excitation spectrum of Sn_2Sb_3 where the emission is fixed at 467 nm and 690 nm. When emission was fixed at 467 nm, an exorbitant peak was observed at 235 nm. When the emission at 690 nm is fixed, a peak at 467 nm is observed which eventually participate in the emission process observed while exiting at 300 and 330nm. emission at 690 nm is fixed, a peak at 467 nm is observed which eventually participate in the emission process observed while exiting at 300 and 330nm.

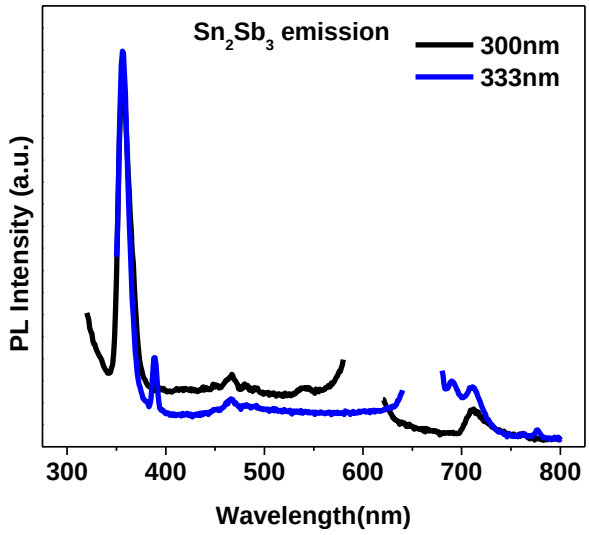

Figure 4.16 (a) Emission Spectrum of Sn_2Sb_3

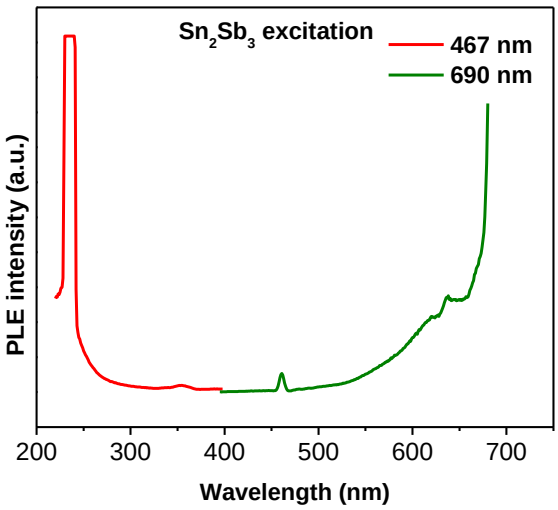

Figure 4.16 (b) Excitation Spectrum of Sn_2Sb_3

The excitation spectrum of the pulverized CuS : Sn_2Sb_3 is shown in the figure 4.18 (a). When the emission is fixed at 345 nm which corresponds to the CuS is taken into account. When emission is fixed at 345 nm, a prospective tricolor emission is observed over a wide range from 515-635 nm which consists of wavelengths 560 nm, 585 nm, 633 nm and other peaks at 469 nm, 482 nm, 492 nm was observed. Hence it is highly expected that the most probabilistic dense states of 345 nm yields better results of RGB (Red, Blue, Green) emission.

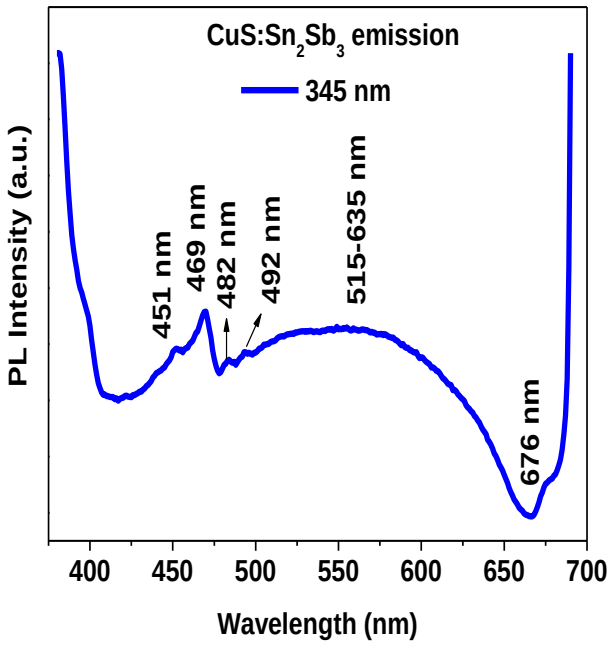

Figure 4.17 (a) Emission Spectrum of pulverized CuS : Sn_2Sb_3

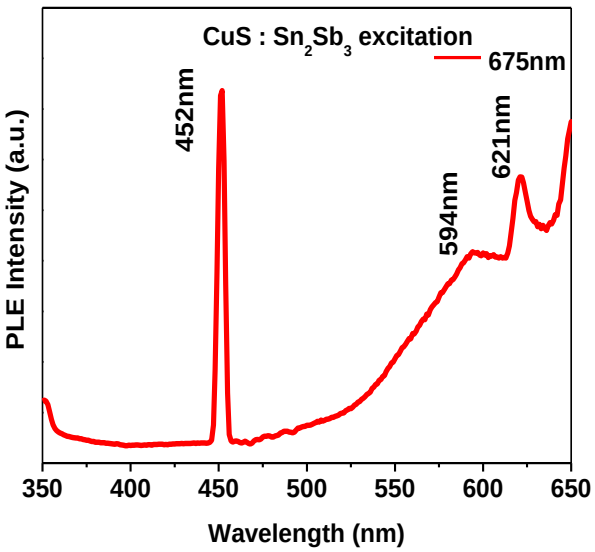

Figure 4.17 (b) Excitation Spectrum of pulverized CuS : Sn_2Sb_3

Figure 4.18 (b) shows the excitation spectrum when emission is fixed at 675 nm, observed a sharp peak at 452 nm, a broad peak at 594 nm and a prominent peak at 621 nm. The peaks along 459 nm, 471 nm, 477 nm, 487 nm, 495 nm, 500 nm corresponds to the closely spaced energy levels which is responsible for emissions at 451 nm, 469 nm, 482 nm, 492 nm.

Therefore the wavelength expected for a white light would be 469 nm (Super Blue), 560 nm (Super pure Green), 585 nm (Yellow), 633 nm (Super Red) reveals the positive outcome from this work. Hence it can be concluded that the method of pulverization of CuS into Sn_2Sb_3 alloy without any addition of dopant remains as a good way to improvise a tricolor emission desired for the White-LED applications.

SUMMARY AND CONCLUSION

CHAPTER V

SUMMARY AND CONCLUSION

CuS and Sn_2Sb_3 are prepared by Co-Precipitation method. The prepared samples are analysed for structural using XRD and elemental composition using EDX which confirmed hexagonal structure and the composition as $Cu_{0.75}S_{1.5}$. And both the samples are pulverized in the ratio of 1:1 for 1000 subsequent rotations. As CuS and Sn_2Sb_3 exhibited hexagonal crystal structure, the hindrances caused due to the multiphase composition in intercalation application is expected to be devoid. When CuS is annealed at 500˚C, drastic changes are noted. TG-DTG analysis of CuS shows that the sample decomposes at 284˚C, in the pulverized sample, no drastic oxidation or recrystallisation had occurred and the process of pulverization of two compounds prevents oxidation and adds value over stabilization process of these compounds. The SEM image obtained for CuS, Sn_2Sb_3 showed well defined spherical structures and few ratio of nanorod or flakes in the case of CuS. On higher magnification, indication spherical, particles, flakes and rods were observed. A non-stoichiometric of the compound also showed a stable structure. All the samples are subjected to FTIR analysis and the results are satisfactory with characteristic peaks assigned with only meagre surfacial oxygen. The pulverized sample had no surfacial oxygen bonding of any of the cationic elements thus indicating the attainment of stability of these two compounds on pulverization. Hence FTIR confirms the charge neutrality of the compounds. UV-Visible analysis shows the absorption spectrum for all the samples, and the band gap obtained by the Tauc - plot for CuS, Sn_2Sb_3 and CuS : Sn_2Sb_3 are 2.50 eV, 3.50 eV and 2.80 eV which is an intermediate value between the band gap values of CuS and Sn_2Sb_3. The photoluminescence analysis are observed for all the samples, and in the pulverized sample CuS and Sn_2Sb_3 showed emission over the visible region and hence showed probabilistic dense states at 345 nm yielding better results of RGB (Red, Green, Blue) emission. It is noteworthy to state that this is the simplest method and prospectively first time achievement towards a novel approach of generating tricolor emission for White light using alloy compounds.

REFERENCES

REFERENCES

1. Sergey Izotov, Anton SItdikov, Vasily Soldatkin, Vasily Tuev, Artem Olisovets; Study of Phosphors for White LEDs; Procedia Technology, Volume 18, 2014, Pages 14-18.

2. Yahong Jin, Yang Lv, Yihua Hu, Li Guifang JU, Zhongfei Mu; Tunable blue-green color emitting phosphors $Sr_3YNa(PO_4)_3F:Eu^{2+},Tr^{3+}$ based on energy transfer for near-UV white LEDs; Journal of Luminescence, Volume 185, 2017, Pages 106-111.

3. Shigeo Shinoya, William M. Yen; Phosphor Handbook, CRC Press Laser and Optical Science and Technology, 2nd Edition, 2006.

4. Su Zhang, Jipeng Fu, Ran Pang and Chengyu Li; Synthesis and Photoluminescence Properties of a Red-Emitting Phosphor $Sr_9Mg_{1.5}(PO_4)_7:Eu^{3+}$; Volume 51, 2016, Pages 50-55.

5. Christian Sommer, Paul Hartmann, Peter Pachler, Hans Hoschopf, Franz P. Wenzlri Karha and Erkki Ikonen; White light quality of phosphor converted light-emitting diodes: A phosphor materials perspective of view; Journal Science and Application: Volume 4, 2015, Pages 105-108

6. Thomas Justel, Hans Nikol and Cees Ronda; New Development in the field of Luminescent Materials for Lighting and Displays; Volume 37, 1998, Pages 3084.

7. Hans Riesen and Zhiqiang Liu; Optical Storage Phosphors and Materials for Ionizing Radiation, Ed : Intech, 2012, Pages 625-648.

8. David. S. Ginley, David Cahen; Fundamentals of materials for Energy and environmental Sustainability, Materials Research Society, 2012, Pages 480-481.

9. Enhanced performances of AlGaInP-based light emitting diodes with Schottky current blocking layers; Chinese Physics B, Volume 24, 2015.

10. Thermally activated degradation of Remote Phosphors for Application in LED lighting, Volume 13, 2012. DOI: 10.1109/ TDMR.2012.2214780.

11. P.C. Schmidt, D.Stahl, B.Eisenmann, R.Kneip, V.Eyert, J.Kubler; Electronic structure of the layered compounds K[SnSb], K[SnAs], K [SnAs] and Sr [SnAs]; Journal of solid state chemistry, Volume 97, 1992, Pages 93-104.

12. V.P. Vasil'ev; A Complex study of the Phase diagram of the Sn-Sb System; Journal of Physical Chemistry, Volume 79, 2003, Pages 20-28.

13. Lavinia Balan, Raphel Schneider, Denis Billaud Jacques Lamert, Jaafar Ghanbaja; A novel solution-phase and low-tesmperature synthesis of SnSb nano-alloys, Volume 59, 2005, Pages 2898-2902.

14. H.T. Zhang, G. Wu, X.H. Chen; Controlled synthesis and characterization of covellite (CuS) nanoflakes; Materials Chemistry and Physics, Volume 98, 2006, Pages 298-303.

15. Keitaro Tezuka, William C.Sheets, Ryoko Kurihara, Yue Jin Shan, Hideo Imoto Tobin Marks, Kenneth R.Poeppelmeier; Synthesis of covellite (CuS) from the elements; Solid State Sciences 9,2007,Pages 95-99.

16. NAN, Zhao-Dong, WANG, Xue-Ying, HAO, Hai-Yan; Self-assembly of Copper Sulphide Nanoparticles to solid, Hollow Spherical and Wire-Shaped Structures; Chinese Journal of Chemistry; Volume 26,2008,Pages 1395-1400.

17. Fei Wang, Mingshu Zhao, Xiaoping Song; The improved electrochemical performance of SnSb-based alloy anode materials for Li-ion batteries, Journal of Alloys and Compounds, Volume 472, 2009, Pages 55-58.

18. Miao Chen, Jing Zhao, Xiaocui Zhao; Scanning electrochemical microscopy studies of micropatterened copper sulphide (Cu_xS) thin films fabricated by a wet chemistry method; Electrochimica Acta, Volume 56, 2011, Pages 5016-5021.

19. Yechang Li, Lei Zhang, Jimmy C.Yu, Shu-Hong Yu; Facet effect of copper (I) sulphide nanocrystals on photoelectrochemical properties; Progress in Natural Science; Material International, Volume 22,2012, Pages 585-591.

20. Joyjit Kundu and Debabrata Pradhan; Influence of precursor concentration, surfactant and temperature on the hydrothermal synthesis of CuS: structural, thermal and optical properties; NewJ.Chem; Volume 37, 2013.

21. Anxiang Wang, Yifu Li, Bin Yang, Baoqiang Xu, Lingxin Kong, Dachun Liu; Process optimization for vacuum distillation of SnSb alloy by response surface methodology, Volume 109, 2014, Pages 127-134.

22. P. Nithyadharseni, B. Nalini, P. Saravanan; Electrical and magnetic effect of transition metals in SnSb nanoalloy, Applied Surface Science, Volume 311, 2014, Pages 503-507.

23. F.Ghribia, A. Alyamanib, Z.Ben Ayadia, K.Djessasc, L.EL Mira; Study of CuS Thin Films for Solar Cell Applications sputtered from Nanoparticles Synthesized by hydrothermal route; Energy Procedia; Volume 84,2015,Pages 197-203.

24. Alok Singh, R.Manivannan, S.Noyel Victoria; Simple one-pot sonochemical synthesis of copper sulphide nanoparticles for solar cell applications; Arabian Journal of Chemistry; 2015.

25. M.Nafees, M.Ikram, S.Ali; Thermal behaviour and decomposition of copper sulphide nanomaterial synthesized by aqueous sol method; Digest Journal of Nanomaterials and Biostructures; Volume 10, 2015, Pages 635-641.

26. P.Nithyadharseni, M.V. Reddy, B.Nalini, M.Kalpana, B.V.R. Chowdari; SnSb-based Intermetallic alloy anode materials for the application of Lithium ion batteries, Electrochimica Acta, Volume 161, 2015, Pages 261-268.

27. Poulomi Roy and Suneel Kumar Srivastava; Nanostructured copper sulphides: synthesis, properties and applications, CrystEngComm, Volume 17, 2015,Pages 7801-7815.

28. Peter A. Ajibade, Nandhipa L.Botha; Synthesis and structural studies of copper sulphide nanocrystals; Results in Physics, Volume 6, 2016, Pages 581-589.

29. Sana Riyaz, Azra Parveen, Ameer Azam; Microstructural and optical properties of CuS nanoparticles prepared by sol-gel route; Perspective in Science; Volume 8, 2016, Pages 632-635.

30. N.Ali, A.Hussain, R.Ahmeda, W.N. Wan Shamuria, Y.Q.Fuc; Synthesis and characterization of copper antimony tin sulphide thin films for solar cell applications; Applied Surface Science; Volume 390, 2016, Pages 393-398.

31. D.Lakshmi, B.Nalini; Performance of SnSb : Ce,Co alloy as anode for lithium-ion batteries; J Solid State Electro chem, Volume 21, 2017, Pages 1027-1034.

32. Charles P.Poole, Jr., Frank J.Owens, Introduction to Nanotechnology, Wiley Interscience, 2003, A John Wiley 81 Sons, Inc., Publication.

33. NAN, Zhao-Dong, WANG, Xue-Ying, HAO, Hai-Yan; Self-assembly of Copper Sulphide Nanoparticles to solid, Hollow Spherical and Wire-Shaped Structures; Chinese Journal of Chemistry; Volume 26,2008,Pages 1395-1400.

34. Ashish Chauhan and Priyanka Chauhan; Powder XRD Technique and its Applications in Science and Technology, Chauhan and Chauhan, J Anal Bioanal Tech, Volume 5, 2014.

35. Charsley E.L. and Warrington S.B., Thermal Analysis: Techniques and Applications, Royal Society of Chemistry.

36. Colin N. Banwell and Elaine M. Mccash; Fundamentals of Molecular Spectroscopy, McGraw-Hill, 1976, Fourth Edition.

37. Barbara H. Stuart, Infrared Spectroscopy: Fundamentals and applications, John Wiley and Sons Ltd., 2004.

38. M.T. Postek, K.S. Howard, A.H. Johnson and K.L. McMichael; Scanning Electron Microscopy: A Student's Handbook, (Ladd Research Ind., Inc. Williston, VT.,), 1980.

39. Andres Kaech; An Introduction to Electron Microscopy Instrumentation, imaging and preparation, University of Zurich, Center for Microscopy and Image Analysis,2012.

40. Joseph. R Lakowicz, Principles of Fluorescence Spectroscopy, Springer Science and Business Media, 2007.

41. Claudia Maria Simonescu, V. S. Teodorescu, Oana Carp, Luminita Patronand Camelia Capatina, Thermal Behaviour of CuS (Covellite) obtained from Copper Thiosulfate system, Journal of Thermal Analysis and Calorimetry, Volume 88, 2007, Pages 71–76.

42. Near Infrared Radiation Absorption Properties of Covellite (CuS) using first-principles calculations, AIP advances, 2016, Volume 6, DOI : 10-1063/1.4962299.

43. Dean W. Sheibley and Maurice H. Fowler Lewis; Infra red spectra of various Metal oxides in the region of 2 to 26 microns, National Aeronautics and Space Administration U.S.A, NASA Technical Note, 1966.